HHS Public Access

Author manuscript

J Mol Biol. Author manuscript; available in PMC 2022 August 06.

Published in final edited form as:

J Mol Biol. 2021 August 06; 433(16): 166991. doi:10.1016/j.jmb.2021.166991.

Molecular mechanism of Nramp-family transition metal transport

Aaron T. Bozzi[#], **Rachelle Gaudet**[*]

Department of Molecular and Cellular Biology, Harvard University, 52 Oxford Street, Cambridge, MA 02138, USA

Abstract

The Natural resistance-associated macrophage protein (Nramp) family of transition metal transporters enables uptake and trafficking of essential micronutrients that all organisms must acquire to survive. Two decades after Nramps were identified as proton-driven, voltage-dependent secondary transporters, multiple Nramp crystal structures have begun to illustrate the fine details of the transport process and provide a new framework for understanding a wealth of preexisting biochemical data. Here we review the relevant literature pertaining to Nramps' biological roles and especially its conserved molecular mechanism, including our updated understanding of conformational change, metal binding and transport, substrate selectivity, proton transport, proton-metal coupling, and voltage dependence. We ultimately describe how the Nramp family has adapted the LeuT fold common to many secondary transporters to provide selective transition-metal transport with a mechanism that deviates from the canonical model of symport.

Graphical Abstract

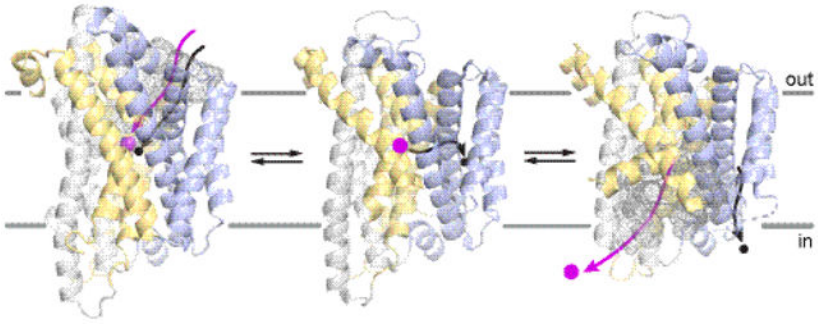

[*]To whom correspondence should be addressed: Rachelle Gaudet: Department of Molecular and Cellular Biology, Harvard University, 52 Oxford Street, Cambridge, MA 02138, USA; gaudet@mcb.harvard.edu; Tel. (617) 495-5616.

[#]Present address: Alexion Pharmaceuticals, 100 College St, New Haven, CT 06510

Aaron T. Bozzi: Conceptualization, Investigation, Writing - Original Draft, Visualization.

Rachelle Gaudet: Writing - Review & Editing, Visualization, Supervision, Project administration, Funding acquisition.

Declaration of interests

The authors declare that they have no known competing financial interests or personal relationships that could have appeared to influence the work reported in this paper.

Keywords

iron homeostasis; manganese; APC superfamily; proton-coupled transport; secondary transporter

Introduction

Organisms must access a sufficient environmental source for each of the two dozen or so essential chemical elements for survival, growth, and reproduction. All lifeforms rely on transition metals to serve as cofactors in enzymes that catalyze many chemical reactions in cellular metabolism and respiration. These transition metal cations—typically manganese (Mn), iron (Fe), cobalt (Co), nickel (Ni) copper (Cu), zinc (Zn), molybdenum (Mo), and tungsten (W)— form semi-covalent bonds with specific electron-donating functional groups in proteins or small organic molecules, thus stabilizing certain folds and imparting chemical properties absent from nature's amino acid repertoire.

The most widely exploited transition metal in biology, iron easily cycles between the Fe^{2+} and Fe^{3+} oxidation states, making it an ideal cofactor for redox (electron-transfer) reactions and thus an essential nutrient for all but a handful of known organisms [1–3]. In addition, iron-sulfur clusters and iron-containing cytochromes provide the pathway for the electron transport in mitochondria that enables efficient ATP generation, while heme iron is used, for example, by globin proteins to transport and store oxygen. Copper and manganese are also widely employed in biological redox reactions, with manganese cofactors famously facilitating photosystem II's oxidation of water to diatomic oxygen. In contrast, the redox-inactive zinc often fulfills a structural role in many proteins or acts as a Lewis acid in enzyme active sites.

Transition metal ions' low solubility in oxygenated water renders these elements scarce in most biological environments [4], creating a thermodynamic challenge for organisms, as concentrating a rare chemical resource in a small membrane-bound compartment such as a cell is entropically unfavorable. To circumvent this obstacle, evolution provided two distinct mechanisms known as primary and secondary active transport. In primary active transport, membrane proteins bind desired substrates and translocate them across the lipid bilayer by combining or "coupling" that transport process with an unrelated energetically favorable chemical reaction such as ATP hydrolysis, thus providing one mechanism for nutrient uptake against a concentration gradient. Dedicated primary active transport proteins also consume ATP energy to establish gradients of common ions such as Na^+, K^+, H^+, and Cl^-. These gradients, when combined with selective membrane permeability through ion-specific channels, lead to a net charge separation or membrane potential, typically negative intracellularly.

Secondary active transport occurs through proteins that harness these preexisting electrochemical gradients to power the thermodynamically unfavorable transport of a desired substrate, such as the import of a scarce micronutrient. Two basic mechanisms of secondary transport exist: symport, in which a protein moves the driving ion and the intended substrate in the same direction across the membrane, and antiport, in which a protein moves driving and intended substrates in opposite directions, usually in separate steps. Secondary active

transporters evolved to catalyze thermodynamically net-favorable transport reactions by enforcing tight “coupling” mechanisms [5–12]. For these proteins, the transport of the primary and driving substrates are codependent, which serves to prevent deleterious uniport events: either futile cycles that dissipate the driving ion gradient without stimulating uptake of the primary substrate, or potentially worse, “backwards” flux of the primary substrate down its concentration gradient [13, 14]. Both primary active transporters and secondary transporters follow some form of the alternating access model [15], in which the transporter only exposes its substrate binding site(s) to one side of the membrane at a time, in contrast to the fully open pore of a channel that allows unfettered substrate movement. The Natural resistance-associated macrophage protein (Nramp) family represents a conserved strategy for acquiring and trafficking essential transition metal ions [16–21]. Conserved throughout the tree of life, Nramp family members transport essential transition metal micronutrients across cellular membranes (Figure 1). Bacterial homologs scavenge environmental Mn^{2+} and frequently aid pathogens in host colonization, while plant and fungal Nramps enable uptake and trafficking of Mn^{2+} and Fe^{2+}. Mammals express two Nramp homologs: NRAMP1, which contributes to the innate immune system’s metal-withholding defense by extracting essential metals from phagosomes to help kill engulfed pathogens, and NRAMP2, which facilitates both dietary iron uptake and the systemic distribution of iron that supplies red blood cell precursors. Naturally occurring mutations to NRAMP1 increase susceptibility to certain infections [19, 22, 23] while those to NRAMP2 frequently cause anemia [24–27]. In this review, we integrate the previous biological and biochemical data with the recent structural and biochemical analyses of bacterial Nramps to flesh out our current mechanistic understanding of this important class of secondary transporters.

Nramps evolved to fulfill crucial roles in maintaining cellular and organismal metal homeostasis

Nramps share a common ancestor—and thus a common tertiary structure, the LeuT fold first seen in a bacterial amino acid transporter [28]—with the myriad transporters of small organic molecules in the Amino Acid-Polyamine-Organocation (APC) superfamily [20, 29, 30]. Nramp transporters likely diverged well before the appearance of eukaryotes, as Nramp homologs are found throughout the tree of life [31]. The Nramp family subdivides into several distinct evolutionary clades (Figure 1). Clades A, B, and C comprise prokaryotic Nramp homologs, with clade B perhaps diverging from the others first, followed by clade A [20, 31, 32]. Prokaryotic clade C may be somewhat more closely related to eukaryotic Nramps, which further subdivide into three distinguishable clades consisting primarily of fungal, plant, and animal homologs [20, 31, 33]. Within the Solute Carrier classification of eukaryotic transporters, Nramps form the SLC11 family. The Nramp family displays a high level of sequence conservation—approximately 25–35% sequence identity from bacterial to mammalian homologs (Figure 2(b))—relative to the evolutionary time over which these proteins have diverged [16, 20]. This conservation likely reflects the selective pressure to preserve a successful biochemical mechanism that fulfills the same basic function of transporting metal ions across cellular membranes in a diverse range of biological contexts.

Functional studies have demonstrated essential metal transport roles for Nramp homologs in numerous bacterial species, both Gram-negative and Gram-positive [34–49]. These proteins are expressed in the inner membrane where they catalyze the uptake of rare transition metals. With prokaryotes often using alternative uptake systems to secure iron and zinc, the most important physiological substrate for Nramps is manganese (which leads to the common protein name for bacterial Nramps: MntH, or H^+-driven Mn^{2+} transporter). Nramp knockout strains accumulate lower total manganese and struggle to grow in manganese-limited conditions [35, 39, 40, 45, 46], and for pathogenic species, often have diminished success at infecting hosts [36, 41, 43, 44, 47, 50]. To help maintain healthy intracellular levels of essential metals—up to ~1 mM total for each metal, most of it protein-bound, with free metal in the low μM range or below—transcriptional regulators such as MntR, Fur, and Zur respond to changes in Mn^{2+}, Fe^{2+}, and Zn^{2+} concentrations, respectively, to control expression of metal importers, exporters, and chaperones [51, 52]. MntR and sometimes Fur typically govern prokaryotic Nramp transcription [53, 54]. In another illustration of the importance of bacterial Nramps, *Lactobacilli* with high expression of an Nramp homolog protect yogurt from spoilage by fungi through competitive exclusion by depleting the manganese supply [55].

Eukaryotes deploy Nramp homologs for two broad purposes: acquiring and distributing sufficient transition metals to meet their own needs and restricting access of pathogens to these nutrients to starve potential invaders (Figure 1(a)). Indeed, these complementary roles may have originated in the earliest single-celled eukaryotes, with Nramps evolving as a mechanism to simultaneously kill bacterial prey and acquire essential nutrients [20], as is observed for the amoeba *Dictyostelium discoideum* [56–58]. Plants typically express multiple homologs: *Arabidopsis thaliana* has six distinct Nramps, and rice (*Oryza sativa*) has seven [59–61]. Plant Nramp homologs enable uptake of Fe^{2+} and especially Mn^{2+} from the soil and subsequent metal distribution to various tissues, as well as vacuolar storage of excess metal ions, thus facilitating growth in low metal conditions [61–69], while also aiding in defense against pathogens through metal withholding to impede infection [64, 66]. Some plants have also adapted Nramp genes to facilitate transport of the non-transition-metal aluminum (Al^{3+}) [70, 71] and incorporated them as the integral membrane portion of a sensor for the phytohormone ethylene [72]. Fungi similarly employ multiple Nramp homologs for environmental metal scavenging and intracellular storage of Mn^{2+} and Fe^{2+} [18, 73–77]. In fish and many invertebrates, a single or two nearly identical Nramp homologs often perform both the innate-immune and metal-acquisition roles [78–80]. In contrast, in higher vertebrates two distinct paralogs—with 62% sequence identity in humans—perform these separate roles, with NRAMP1 (also known as SLC11A1) specializing in the innate immune system's metal-withholding response to infection, and NRAMP2 (also known as DMT1, or Divalent Metal Transporter 1, and SLC11A2) enabling dietary uptake and facilitating systemic distribution of essential metals (Figure 1(a)) [21, 33, 81–85].

In mammals, NRAMP1 is expressed solely in phagocytic cells (Figure 1(a)) [86, 87], where it aids in the killing of engulfed microbes by extracting essential transition metals from the phagosomes [88–90], thus restricting pathogen growth through metal starvation [91] and rendering them more susceptible to damage from the concurrent release of reactive oxygen species (ROS) [92, 93]. An alternative model posits that NRAMP1 instead functions by

importing redox-active metals to phagosomes to catalyze additional ROS generation [94, 95], but this role would require a significant (and unlikely) divergence in transport mechanism. Deleterious mutations in NRAMP1 lead to increased susceptibility to intracellular pathogens such as *Mycobacterium* in mice [87, 96, 97], and polymorphisms in human NRAMP1 are associated with differential rates of bacterial infection [22].

Mammalian NRAMP2 is abundantly expressed in the small intestines, where it transports Fe^{2+} across the apical membrane into the enterocyte cytosol (Figure 1(a)) [17, 98–100]. Within enterocytes, NRAMP2 translation is governed by an iron response element (IRE) sequence in its mRNA [101], which iron-sensing transcriptional regulators bind under high iron conditions to repress translation [102]. The unrelated transporter ferroportin exports Fe^{2+} from the cytosol into the bloodstream [103, 104], where it is immediately oxidized to Fe^{3+} [105], and then tightly binds to transferrin, a blood plasma iron-distribution protein [106]. Destination cells endocytose transferrin into vesicles that are acidified to stimulate Fe^{3+} release, which enables reduction to Fe^{2+} by STEAP3 [107, 108]. Free Fe^{2+} is then transported across the vesicle membrane to the cytosol by an alternate splice variant of NRAMP2 that functions the same as the intestinal isoform [109] but is expressed in essentially all somatic cells and found at the endosomal membranes [110–113]. Erythroblasts in the bone marrow are the major consumers of transferrin-bound iron, with the mitochondria—the location of heme production—the immediate destination for most Fe^{2+} that enters the cytosol through this route (Figure 1(a)) [84]. NRAMP2 likely assists in Fe^{2+} transport across the outer mitochondrial membrane [114–116]. In addition, both NRAMP1 and NRAMP2 participate in the recovery of free Fe^{2+} from phagocytosed senescent erythrocytes [117–119], although most recovered iron is likely in the form of intact heme, which requires an alternative transport mechanism [118, 120].

Deleterious mutations in NRAMP2 typically cause microcytic anemia in rodents [121–124] and humans [24–27, 125, 126]. This condition arises from poor absorption of dietary iron in the intestines as well as poor distribution of iron to red blood cell precursors, and results in erythrocytes deficient in mature hemoglobin [122]. NRAMP2 mutations may also cause liver iron overload [25, 27], although perhaps indirectly rather than because of an essential NRAMP2 role in hepatocytes [127]. Mice that completely lack the NRAMP2 gene die from severe iron shortage shortly after birth [127], while those lacking only intestinal NRAMP2 suffer from chronic iron deficiency [128].

Nramp homologs thus play critical roles in maintaining metal homeostasis in numerous biological contexts from bacteria to man. This review will update our understanding of the common transport mechanism of the Nramp family [20, 21, 129–131], exploiting the recent crystal structures from three prokaryotic homologs as well as functional studies from over the course of the more than two decades since these proteins were first identified as transition metal transporters.

Nramp model systems

The most extensively studied Nramp homologs are human (*Homo sapiens*), mouse (*Mus musculus*), and rat (*Rattus norvegicus*) NRAMP2 (DMT1), which are all > 90% identical in

sequence (Figure 1); budding yeast (*Saccharomyces cerevisiae*) Smf1p; and bacterial MntH homologs from *Escherichia coli* (which we will refer to as EcoliNramp); *Deinococcus radiodurans* (DraNramp); *Staphylococcus capitis* (ScaNramp); and *Eremococcus coleocola* (EcoleNramp). An alignment of these model systems' primary sequences is provided in Figure 2. As our model system DraNramp currently has the most comprehensive structural information available (crystal structures at four stages of the transport cycle) as well as significant functional and mutagenesis data [132–136], that homolog will be used as the reference sequence, such that when residues or mutants in other homologs are discussed, the corresponding residue number for DraNramp will follow in parentheses.

Nramps adapt a common secondary transporter fold to a unique conformational change mechanism

Nramps typically consist of 11 or 12 transmembrane (TM) α-helical segments [16]. *In vivo* studies with EcoliNramp β-lactamase and chloramphenicol acetyltransferase fusions [137] and human NRAMP2 using inserted hemagglutinin tags [138] confirmed the expected topology and an intracellular N-terminus. Crystal structures of *Staphylococcus capitis* (Sca) Nramp [139], *Deinococcus radiodurans* (Dra) Nramp [134, 136], and *Eremococcus coleocola* (Ecole) Nramp [140, 141] demonstrated a LeuT fold [28] for this protein family, as was previously predicted based on distant sequence homology [20, 142, 143]. This fold, common to many secondary transporters and first observed in the eponymous amino acid secondary transporter from *Aquifex aeolicus* [28], consists of ten TMs, divided into two pseudosymmetric, interlocking repeats of five consecutive TMs (1–5 and 6–10 for Nramp, Figure 2(a)), with the first TM of each repeat broken into two helices (1a, 1b and 6a, 6b) by unwound regions that form the primary substrate binding site at the core of the protein. Some notable structural features do however vary among Nramps. First, EcoleNramp and many eukaryotic homologs have a twelfth TM, which DraNramp, ScaNramp, and most prokaryotic homologs lack (Figure 2). Second, ScaNramp, EcoleNramp, and most clade C prokaryotic and eukaryotic Nramps have an extra turn within TM9 absent from DraNramp and clade A prokaryotic homologs (Figure 2(c)). Last, the N-terminus and the loop regions between TMs vary considerably in length among homologs, especially those connecting TMs 5–6, 7–8, and 9–10.

Currently available Nramp structures capture five distinct snapshots of the alternating-access metal transport cycle (Table 1 and Figure 3): outward-open apo (substrate-free) (EcoleNramp and DraNramp), outward-open metal-bound (DraNramp), inward-open metal-bound (ScaNramp), inward-open apo (ScaNramp and DraNramp), and occluded apo (DraNramp). The DraNramp and EcoleNramp outward-open and DraNramp and ScaNramp inward-open structures align well (Cα RMSD of 2.7 and 2.5 Å respectively) despite only moderate sequence conservation (32% and 35% identity respectively), suggesting that similarly diverged homologs such as human NRAMP2 (27% identical to DraNramp) share the same overall secondary and tertiary structure. In the outward-open state, an aqueous vestibule between TMs 1b, 3, 6a, 8, and 10 provides access for divalent cation substrates to the metal-binding site from the outside, while in the inward-open state a separate vestibule opens between TMs 1a, 2, 5, 6b, and 7 to allow metal release to the inside (Figure 3). Tight

sidechain packing seals the inside vestibule in the outward-open state and the outside vestibule in the inward-open state, while in occluded DraNramp the metal-binding site is inaccessible to solvent from either side. We originally referred to this structure as “inward-occluded” because it more closely resembles the inward-open state (Cα RMSD of 1.96 Å) than the outward-open state (Cα RMSD of 3.50 Å). Accessibility measurements to membrane-permeable or impermeable modifiers at single-cysteine substitutions spanning TMs 1, 3, and 6 of DraNramp expressed in *E. coli* confirmed the physiological relevance of these complementary pathways [134]. The transporter is in a dynamic conformational equilibrium in *E. coli* membranes even in the absence of added metal substrate, as cysteines lining either vestibule were fully labeled with the membrane-permeable modifier N-ethylmaleimide within a few minutes at room temperature.

Comparing the outward-open (EcoleNramp, DraNramp), occluded (DraNramp), and inward-open (ScaNramp, DraNramp) structures revealed that TMs 1a, 4, 5, 6a, and 10 reorient the most to effect the conformational change [136, 140], both in relation to the other relatively-stationary TMs and each other [136], which inform the model in Figure 3(b). Starting in the outward-open state, TM6a and TM1b tilt above their respective non-helical hinge regions towards TMs 3 and 8, while the top half of TM10 also topples over a conserved proline to form a ~20 Å barrier of predominantly hydrophobic residues above the metal-binding site. The TM6a movement may be coordinated (through the TM5–6 linker helix) with the rigid reorientation of TM5 helping to open the more hydrophilic inner gate as the transporter reaches the occluded state. To sample the inward-open state, additional displacement of TM4-TM5 releases TM1a to rotate upward perpendicular to the membrane to fully open the inner gate [136] (Figure 3(c)).

Several anemia-causing mammalian NRAMP2 mutations may impair conformational cycling. The ΔV114 (M84 in DraNramp) mutation in human NRAMP2 [25] shifts the registry of TM2 along the intracellular vestibule, while G75R (G45) on TM1a [125] and G212V (G180) on TM5 [25] in human NRAMP2 add steric bulk at positions abutting a highly conserved salt bridge (E176-R244) that links TM5 and TM6b to close the inner gate in the outward-open state. Indeed, G75R eliminated metal transport in human NRAMP2 [134], and the analogous G45R DraNramp cannot sample the outward-open state, as assessed using a single-cysteine reporter lining the external vestibule [134, 136]. G185R (G153) in mouse NRAMP2 or rat NRAMP2 causes microcytic anemia [121, 122] due to severely impaired Fe^{2+} transport and altered protein localization [123, 124, 144]. The analogous mutation in DraNramp similarly impaired transition metal transport and increased the accessibility of the external vestibule while retaining intracellular vestibule accessibility [134].

Additional mutagenesis experiments support the importance of the unfettered movement of TM1a to the metal transport cycle. While replacing the native residues of DraNramp’s TM1a with cysteine in most cases preserved function, pretreatment with the bulky thiol-modifier N-ethylmaleimide (NEM) at positions along TM1a from P46 to A53 eliminated Co^{2+}-transport [134]. In addition, the analogous tryptophan mutants also eliminated metal uptake and prevented the protein from reaching the outward-open state, demonstrating that excessive steric bulk is not tolerated along TM1a [134], likely due to its significant

intramolecular displacement during transport. In contrast, cysteine or alanine replacements along DraNramp's TM6b both impaired or eliminated metal transport, and loss of the native steric bulk also prevented sampling of the outward-open conformation [135]. These results echoed prior work with EcoliNramp in which most substitutions along the highly conserved TM6b also severely reduced metal transport [145], likely also due to altered conformational cycling. Thus, TM6b plays a crucial role in stabilizing the outward-open state in Nramps, likely through helping to first close the inside gate, and the fact that sidechains on all sides are important suggests it may undergo motions not yet captured in the available crystal structures [135]. Furthermore, adding steric bulk through tryptophan mutagenesis on the faces of TM6a and TM10 that line DraNramp's external vestibule, such as the G223W substitution used to trap the protein in the outward-open state for crystallization, also impaired metal transport and internal vestibule opening [136], demonstrating that closing the transporter's outside gate is prerequisite to opening the inside gate, as the alternating access model predicts.

Finally, functional studies with conformationally locked DraNramp mutants suggested that transported protons and transition metal cations follow distinct routes that require separate intramolecular rearrangements (Figure 4). In contrast to metal transport [134, 136], proton uniport occurred through outward-open locked DraNramp variants but not analogous inward-locked variants [136]. Thus, while metal transport requires bulk conformational change, proton transport does not require sampling of the inward-open state. Metal and proton cosubstrates likely enter the protein through the same external vestibule but take separate routes to the cytosol, with metal ions transiting the wide vestibule seen in the inward-open structures but protons traveling a narrower pathway open even in the outward-locked state. However, the mechanism of proton and metal symport, including whether or how the substrates are thermodynamically coupled, remains unclear.

In summary, the Nramp transport mechanism deviates from structurally related LeuT-fold transporters, in which the intended substrate and the driving ion(s) both enter via one vestibule and exit together via another vestibule following bulk conformational change [28, 146–152]. Intramolecular structural rearrangements enable Nramps to cycle through at least three stable conformations: outward-open, occluded, and inward-open. Nramps thus ensure that metal transport occurs through an alternating access process, in which metal substrate may only reach the binding site at the core of the protein from one side of the membrane at a time, thereby preventing channel-like fluxes of metal. In contrast, protons are transported through a separate narrow pathway adjacent to the wider vestibule used for metal release and accessible in the outward-open state in DraNramp without requiring large-scale conformational change, leading to uncoupled proton flux. Furthermore, the required rearrangements of TMs that accomplish conformational change indicate a complex, possibly multistep process, rather than the rotation of a fairly rigid "bundle" domain (TMs 1, 2, 6, and 7) against a stationary "scaffold" (comprising the remaining TMs) that was proposed for other LeuT-fold family members [8, 153]. Thus, a common tertiary fold can be adapted for strikingly different transport mechanisms, in terms of both the pathways taken by the cosubstrates and the identity of the moving pieces that enable alternating access.

Nramps are relatively promiscuous divalent transition metal transporters

In the landmark study that definitively established Nramps as transition metal transporters, Gunshin and colleagues showed that Mn^{2+}, Fe^{2+}, Co^{2+}, Ni^{2+}, Cu^{2+}, Zn^{2+}, Cd^{2+}, and Pb^{2+} (but not Ca^{2+}) stimulated inward currents—presumably from cation entry—in *Xenopus* oocytes expressing rat NRAMP2, while radioactivity measurements directly demonstrated Fe^{2+} transport [17]. Numerous studies [88, 154–161] have confirmed that mammalian NRAMP2 homologs transport Mn^{2+}, Fe^{2+}, Co^{2+}, and Cd^{2+} using radioactive substrate or metal-sensing dyes (Table 2). In most reports, Zn^{2+} transport was observed [155, 158, 161–163] but not others [109, 154]. Reports are conflicting regarding transport of Pb^{2+} [164, 165], Hg^{2+} [161, 166], and Cu^{2+}/Cu^{+} [158, 161, 167]. Surprisingly, vanadium (likely as VO^{2+}) was transported by human NRAMP2, but VO^{+} and other transition metal cations (Fe^{3+}, Cr^{2+}/Cr^{3+}, and Ga^{3+}) were not [161]. Multiple studies have demonstrated that mammalian NRAMP2 homologs do not transport Ca^{2+} [109, 133, 144, 158, 168]. Adding excess Ca^{2+} reduced Fe^{2+}-provoked currents [17] and decreased the Fe^{2+} transport rate twofold without perturbing the K_m for Fe^{2+}, suggesting noncompetitive inhibition [168]. Fellow alkaline earth metals Ba^{2+}, Sr^{2+}, and to a lesser degree Mg^{2+}, had similar effects on Fe^{2+} transport [168].

Mammalian NRAMP1 homologs have similarly been shown to transport Mn^{2+}, Fe^{2+}, Co^{2+} and Zn^{2+} [88, 90, 94]. Intriguingly, a recent study provided evidence that while functional mouse NRAMP1 expression indeed depleted phagosomes of Fe^{2+} and Zn^{2+}, it also induced a Mg^{2+}-starvation response in *Salmonella* intracellular pathogens [91]. This finding suggests that NRAMP1 could also transport that essential alkaline earth metal, which could perhaps enhance its antimicrobial potency.

Other Nramps have a similar substrate profile, as evidenced by observed Mn^{2+}, Fe^{2+}, Co^{2+}, Ni^{2+}, Zn^{2+}, and Cd^{2+} transport in fungal homologs *S. cerevisiae* Smf1p [74, 75, 169] and *Cryptococcus neoformans* NRAMP1 [73], and in protist *D. discoideum* NRAMP1 [170]. For plant homologs, Nramps from *A. thaliana* transport Mn^{2+}, Fe^{2+}, Zn^{2+}, and Cd^{2+} [61–63, 171, 172], while *Thlaspi japonicum* NRAMP4 was implicated in Ni^{2+} accumulation [173], and overexpression of an *O. sativa* NRAMP1 increased arsenic (As^{3+}) uptake [174]. But buckwheat FeNramp5 transported Mn^{2+} and Cd^{2+} but little Fe^{2+} when expressed in yeast [175]. Interestingly, a tunicate *Ascidia sydneiensis samea* Nramp mediated VO^{2+} uptake, a process which the divalent first-row transition metals inhibited to varying degrees [176], suggesting vanadium may indeed be a viable substrate for many Nramp homologs [161].

Among prokaryotic Nramps, Mn^{2+}, Fe^{2+}, Ni^{2+}, Co^{2+}, Zn^{2+}, and Cd^{2+} transport was demonstrated for EcoliNramp [37, 38, 133, 142, 177, 178] as was discrimination against Ca^{2+} and Mg^{2+} [37]; Mn^{2+}, Fe^{2+}, Co^{2+}, Ni^{2+}, and Cd^{2+} transport was shown for ScaNramp [133, 139] along with discrimination against Ca^{2+}, Ba^{2+}, and Sr^{2+} [139]; and robust Mn^{2+}, Fe^{2+}, Co^{2+}, Zn^{2+}, and Cd^{2+} transport compared with only slight Ca^{2+} uptake was seen for DraNramp [132, 133] along with significant discrimination against Ca^{2+} and Mg^{2+} [133, 134]. Recent electrophysiology measurements showed that *Enterococcus faecalis* MntH2 transported Mn^{2+}, Co^{2+}, Zn^{2+}, Cd^{2+}, but little to no Cu^{2+}, Fe^{2+} or Ni^{2+} [179]. Prokaryotic

and eukaryotic Nramps therefore generally transport the same divalent transition metal substrates while rejecting divalent alkaline earth metals and nondivalent transition metals.

Numerous studies reported a similar K_m (or $K_{0.5}$) in the range of 1–5 μM for mammalian NRAMP2 homologs for the biological substrate Fe^{2+} [17, 88, 109, 156, 157, 161, 165, 180] (Table 3). Mn^{2+}, Co^{2+}, and Cd^{2+} transport occurred at similar K_m [88, 139, 161], with Zn^{2+} and Ni^{2+} transported at approximately an order-of-magnitude higher K_m (10–30 μM) [161, 162, 180]. Yeast Smf1p has similar K_m values for Mn^{2+}, Fe^{2+}, and Co^{2+} transport [74, 169] as mammalian NRAMP2 homologs.

Prokaryotic Nramps transport their physiological substrate Mn^{2+} with a similar K_m, although a broader range of values have been reported: 0.1–1 μM for EcoliNramp and the nearly-identical *Salmonella enterica* serovar Typhimurium Nramp [37, 145, 178, 181], 2–3 μM for DraNramp [132, 136], and 20 μM for EcoleNramp [140]. EcoliNramp [142] and DraNramp [132, 136] also efficiently transport Cd^{2+} (K_m < 10 μM), while K_D measurements for Cd^{2+} yield a similar range for DraNramp (10 μM) [133] and ScaNramp (30 μM) [139]. Interestingly, DraNramp transports Zn^{2+} (30 μM), Fe^{2+} (200 μM), and Co^{2+} (700 μM), with markedly higher K_m [133]. EcoliNramp and *S.* Typhimurium Nramp showed similar trends favoring Mn^{2+} and Cd^{2+} over other divalent metals in growth-inhibition and transport competition experiments [37, 38]. Bacterial homologs may thus have evolved higher specificity for their intended substrate Mn^{2+} along with incidental high Cd^{2+} affinity, while eukaryotic Nramps generally retain similar high affinities for Mn^{2+}, Fe^{2+}, Co^{2+}, Zn^{2+}, and Cd^{2+}, although the structural basis or sequence signature of this differentiation remains unknown.

To recap, the Nramp family evolved to provide high-affinity ($K_m \approx 1$ μM) transmembrane transport of the micronutrients Mn^{2+} and Fe^{2+}, their primary biologically relevant substrates in most organisms. The K_m of Nramps for their physiological substrates Mn^{2+} and Fe^{2+} likely exceeds their concentrations by an order of magnitude or more in many environments. This relatively high K_m, although in a comparable range to many unrelated metal transporters, may be a trade-off necessary to enable timely metal release to the cytosol, which a significantly higher-affinity site might delay. However, Nramps are highly promiscuous regarding substrate choice and transport numerous divalent transition metals, including the biologically useful Co^{2+}, Ni^{2+}, and Zn^{2+}, as well as the toxic Cd^{2+} and perhaps other heavy metals. The notable promiscuity of Nramps amongst transition metals in part reflects the challenges of engineering a highly selective Mn^{2+}- or Fe^{2+}-binding site. Similar-sized transition metal ions usually compete for the same binding site, and their differing electronic properties often cause Co^{2+}, Ni^{2+}, Zn^{2+}, and Cd^{2+} to interact more strongly with a given set of coordinating ligands than do Mn^{2+} or Fe^{2+}, as described by the Irving-Williams series [51, 52, 182]. Given that these and other transition metals are typically even rarer environmentally than iron and manganese, there may not have been significant selective pressure for Nramps to further tune the geometry or amino acid composition of the metal-binding site to allow only Mn^{2+} or Fe^{2+} transport. In contrast, the alkaline earth metals like Ca^{2+} and Mg^{2+} are abundant in most environments, and therefore robust discrimination by most Nramps against these non-transition metal cations likely reflects an essential adaptation to obtain scarce micronutrients.

Structural insights into Nramp metal ion binding, transport, and selectivity

Nramps use a highly conserved metal-binding site located within the unwound regions of TMs 1 and 6; this location of the binding site for the main cargo substrate is a conserved feature of the LeuT fold [29]. Ehrnstorfer and colleagues provided the first snapshot of an Nramp metal-binding site in ScaNramp's inward-open state [139] (Figure 5(b)). In this structure, sidechains D49 (D56) and N52 (N59) from TM1, and sidechain M226 (M230) and the A223 (A227) backbone carbonyl from TM6, coordinate the Mn^{2+} substrate, although the resolution is too low to confidently assign the coordination sphere geometry or identify any ordered waters that would perhaps complete it. In crystals soaked with other potential substrates, the metal cations Fe^{2+}, Co^{2+}, Ni^{2+}, Cd^{2+}, and Pb^{2+} all bound at same site as Mn^{2+}, while Cu^{2+} shifted somewhat in location but retained a close interaction with M226 [139]. In contrast, Zn^{2+} surprisingly bound in another site entirely, interacting closely with TM6b's H233 (H237) along the metal release pathway, while the alkaline earth metals Sr^{2+}, Ba^{2+}, and Ca^{2+} also did not bind to the Mn^{2+} site, even when soaked at 200 mM [139].

A complementary structure from DraNramp in the outward-open state showed TM1's D56, N59, and A53 carbonyl, along with TM6's M230—but not A227—and two ordered waters coordinating a Mn^{2+} with an octahedral-like geometry [136] (Figure 5(a)). In addition, in an apo-occluded structure of DraNramp the highly-conserved Q378 from TM10 approaches the other metal-binding residues, suggesting it could transiently coordinate metal substrate in a metal-bound intermediate conformation [136], an interaction that two independent molecular dynamics simulations with ScaNramp also predicted [133, 157]. Comparing all available structures, the Nramp metal-transport cycle appears to require a transition from four (D56, N59, M230, A53) to five or six (adding A227 and possibly Q378) to four (removing A53 and Q378) Mn^{2+}-coordinating residues (Figure 5(c)). These changes to the metal coordination sphere may serve to provide a coordination geometry that favors the transition state [10], thereby lowering the energy barrier for transport. Furthermore, to achieve the hypothetical intermediate five- or six-residue Mn^{2+} coordination, TM6a and TM10 must reorient to close the external vestibule, perhaps helping to trigger the essential bulk conformational changes that ultimately allow opening of the cytosolic vestibule and metal release.

Numerous mutational studies have validated the importance of the observed metal-binding residues to transport by Nramps (Figure 5(d) and Table 4). Either alanine or more conservative substitutions for the TM1 aspartate and asparagine (D56 and N59) impaired Cd^{2+} binding to ScaNramp [139] and eliminated or severely reduced metal transport in human NRAMP2 [133, 139, 183], EcoliNramp [133, 177, 178, 181], EcoleNramp [140], and DraNramp, for which the N59D mutation—but not N59A, D56A, or D56N—preserved some transport [133, 135, 136]. These two metal-coordinating residues thus appear essential to the general Nramp transport mechanism, such that no metal substrate will bind without a suitably placed sidechain ligand in these positions.

The conserved metal-binding TM6 methionine (M230 in DraNramp) also plays a crucial role in metal transport and in determining Nramp substrate selectivity. In human NRAMP2, M-to-A, -C, and -Q mutations eliminated all metal transport [133, 139, 157], while an M-to-

A switch also eliminated Fe^{2+} transport in the protist *Perkinsus marinus* Nramp [184]. An M-to-A mutation at this position impaired Cd^{2+} binding and metal transport in ScaNramp [133, 139] and reduced Mn^{2+} transport in EcoleNramp [140], as did M-to-I and -K mutations in EcoliNramp [145]. For DraNramp, mutation of M230 to alanine or other small amino acids (G/S/T/C) preserved transport of Fe^{2+} and Co^{2+}—as well as Mn^{2+} (albeit with a 40-fold higher K_m for M230A than WT [132])—but increased susceptibility to competition from excess Mg^{2+} and Ca^{2+} [133]. In addition, M230A enabled significant transport of Ca^{2+} and rendered overexpressing *E. coli* more susceptible to Mg^{2+} and Ca^{2+} toxicity than the WT counterpart [133]. In contrast, the M230A mutation severely impaired the binding and transport of Cd^{2+} [133], resulting in a 300-fold increase in K_m compared to the WT [132], thus conferring greater tolerance to Cd^{2+} toxicity in *E. coli* [133]. These results suggest that the thioethyl sulfur of the methionine—the lone non-oxygen in the metal's inner coordination sphere—interacts in a semi-covalent manner to preferentially stabilize transition metal substrates, Cd^{2+} in particular. In contrast, alkaline earth metals Mg^{2+} and Ca^{2+}, which interact solely in an ionic manner and thus prefer the more electronegative oxygen as a ligand, only become viable substrates when the methionine is truncated to alanine—thus leaving room for a water molecule to remain bound to the metal—or replaced by a hydroxyl-bearing residue such as threonine. Indeed, bacterial Nramp-like Mg^{2+} transporters exchange the metal-binding methionine for threonine [185], as does an Nramp-related aluminum transporter (Nrat1) from *O. sativa* that favors the non-transition metal cation Al^{3+} [71]. Furthermore, replacing three consecutive TM6 residues in *O. sativa* NRAMP3 including the methionine with their counterparts from Nrat1 enabled Al^{3+} transport by the chimeric protein [186]. Conservation of the TM6 methionine in Nramps therefore likely represents an evolutionary trade-off, whereby the benefit from enabling effective discrimination against the abundant alkaline earth metals overrides the concomitant drawback of increased susceptibility to toxic heavy metal uptake in most environments, with the relative magnitudes of the selective pressures perhaps reversed for some extremophiles native to heavy-metal rich environments that naturally possess the M-to-A change [187].

Residues outside the primary coordination sphere also tune Nramp metal selectivity

Additional mutational studies have identified positions beyond the TM1/TM6 core substrate binding site that contribute to metal specificity, either through forming part of the outer metal-coordination sphere or through allosteric networks connecting them to the metal-binding site (Figure 5(d) and Table 4).

On TM10, A-and Q-replacement of the native N443 (Q378) eliminated transport in human NRAMP2 [157], while in DraNramp Q378A and Q378L greatly impaired transport and hydrophilic replacements Q378S and Q378N retained significant metal transport [135], with the latter two proteins having a comparable-to-WT K_m for Cd^{2+} but an order-of-magnitude higher K_m for Mn^{2+} [136]. As Cd^{2+} typically prefers fewer ligands than Mn^{2+} (or Fe^{2+}) in its coordination sphere, Q378 may only be essential to optimal coordination of Mn^{2+}.

Additional residues that influence metal selectivity can be ascribed to a secondary selectivity sphere that is close to, but not in, the metal-binding site. A screen with *A. thaliana* NRAMP4 identified three mutations that preserved Fe^{2+} transport while improving the Cd^{2+} tolerance of transformed yeast: L67I/V (M55), within the unwound region of TM1 just below metal-binding D56; E401K (I375), one helix turn above proposed metal-binding Q378 on TM10; and F413I (F387), below Q378 on TM10 [171]. Interestingly, while L67I/V and F413I preserved WT-like Fe^{2+}, Mn^{2+}, and Zn^{2+} transport while reducing Cd^{2+} uptake, E401K only provided WT-like Fe^{2+} uptake. The analogous F-to-I mutation on TM10 in rat NRAMP2 largely preserved Fe^{2+} and Mn^{2+} transport but impaired Zn^{2+} and Cd^{2+} uptake [171], further evidence that different substrate metals likely forge distinct interactions during the transport process. These findings illustrate the importance of TM10 and other regions adjacent to the metal-binding site in determining Nramp metal selectivity, likely through shaping the secondary metal coordination sphere.

Mutations in the relatively stationary part of the protein can also influence metal selectivity. The anemia-causing mouse NRAMP2 mutation G185R (G153) [122], located at the extracellular end of TM4 ~20 Å from the metal-binding site, greatly reduced Fe^{2+} transport [124, 144] while surprisingly enabling significant permeability to Ca^{2+}, Ba^{2+}, and Sr^{2+}, and to a much lesser extent Mg^{2+} [144]. The analogous G153R mutation in DraNramp also impaired transport of Fe^{2+} and other transition metals, with the residual transport still dependent on the conserved binding-site residues [134]. This mutation also significantly improved Ca^{2+}—but not Mg^{2+}—transport, and Ca^{2+} competition with Fe^{2+}, in a manner complementary rather than redundant with the M230A mutation [134]. G153 abuts a highly conserved hydrophilic network between TMs 3, 4, 8, and 9 that connects to the metal-binding site and provides the pathway for proton transport (see below) and may also impact substrate specificity. Within this network, mutations to highly conserved E134 and H232 adjacent to metal-binding D56, as well as the more distant D131 and R352, selectively reduced Mn^{2+}- but not Cd^{2+}-transport efficiency compared to WT, while the nearby mutation R353A enhanced Ca^{2+} transport similarly to G153R [132]. Lastly, in rat NRAMP2, the H272A (H237) mutation to a highly conserved histidine on TM6b along the metal-release pathway reduced Fe^{2+} transport efficiency, but left Zn^{2+} transport unaffected, such that both metals were similarly good substrates for the mutant in contrast to the WT's preference for Fe^{2+} [180].

Insights gleaned from Nramp structure-function studies guided the design of yeast Smf1p variants that selectively accumulate Cd^{2+} and Sr^{2+} as part of a strategy for environmental remediation of toxic heavy metal contamination [188]. Combining the M276A (M230) and G169R (G153) mutations that maximized Ca^{2+} uptake in DraNramp [134] enabled Smf1p-expressing yeast to import larger quantities of the similar alkaline earth metal Sr^{2+} [188]. In addition, the M276C (M230) mutation shifted the metal preferences of yeast Smf1p to relatively favor Cd^{2+} over Mn^{2+} transport [188], further underscoring the importance of a sulfur ligand in the binding site to Cd^{2+} selectivity in Nramps [133]. In this study, directed evolution identified additional mutations on TM1 and 6 that altered yeast Smf1p's metal uptake preferences: S105C (R69) and T266S (L220) along the outward metal-permeation pathway improved Sr^{2+} selectivity; S269T (G223), also along the outward vestibule, and

G283Q (H237), along the inward metal-release pathway, both increased Cd^{2+} selectivity [188].

The available Nramp structures have identified residues that directly coordinate metal substrate during transport, with mutagenesis experiments validating these interactions. In addition, functional studies have demonstrated the ability of many additional residues to affect Nramp metal selectivity, either through shaping the secondary metal-coordination sphere or forming long-range allosteric networks that connect to the metal-binding site.

Nramps as secondary active transporters

Active transport is required to overcome concentration gradients as cells hoard the scarce nutrients they extract from their environments. Secondary active transporters harness electrochemical energy from preexisting transmembrane ionic gradients to power the movement of a primary substrate against its own concentration gradient. Nramp transporters may have evolved as proton-metal cotransporters to ensure the thermodynamic favorability of metal import, although in some contexts metal uptake would appear to be favorable on its own. While absolute cytosolic concentrations of Nramp substrates Fe^{2+} and Mn^{2+} can approach 1 mM, most accumulated metal ions are tightly bound to specific proteins, either in enzyme active sites, in essential structural roles, or in designated storage proteins [182]. The free metal concentration is thus significantly lower—typically in the low μM range for Mn^{2+} and Fe^{2+}, but at levels still orders of magnitude higher than ambient concentrations in many environments [51]. Thus, analogous to an enzyme, Nramp transporters may need to redirect cellular energy (from dissipating a proton gradient and membrane potential) to effect an otherwise-unfavorable chemical change.

For a transport reaction involving charged substrates such as the ones DraNramp catalyzes, assuming a 1:1 stoichiometry between metal (M^{2+}) and proton (H^+) cosubstrates:

$$M^{2+}{}_{out} + H^{+}{}_{out} \rightarrow M^{2+}{}_{in} + H^{+}{}_{in}$$

both the M^{2+} and H^+ concentrations and the physiological membrane potential ($\Delta\Psi$) determine the overall thermodynamics (ΔG):

$$\Delta G = RT\ln\frac{\left[M^{2+}\right]_{in}}{\left[M^{2+}\right]_{out}} + RT\ln\frac{\left[H^{+}\right]_{in}}{\left[H^{+}\right]_{out}} + z_{M^{2+}}F\Delta\Psi + z_{H^{+}}F\Delta\Psi$$

where R is the ideal gas constant, T is temperature, F is the Faraday constant, and z is the net charge of each ionic species. The membrane potential alone provides a significant driving force: −27 kJ/mol for a 2+ cation at $\Delta\Psi$ = −140 mV (negative inside), a value typical for prokaryotes [189], which is enough to overcome a 50,000-fold metal concentration gradient. Requiring H^+ cotransport under ΔpH conditions further energetically favors uptake: −21 kJ/mol at ΔpH = 1.5 and $\Delta\Psi$ = −140 mV, which provides for an additional 5,000-fold concentration of M^{2+}. In eukaryotic cells, a typical $\Delta\Psi$ = −70 mV (negative inside) sustains only a 200-fold metal concentration difference, so proton cotransport at ΔpH = 1.5 that

enables an additional 400-fold concentration is likely more consequential physiologically. However, these large contributions to the net thermodynamics do not require that ΔΨ and pH also affect the transporter's kinetics, which depend only on the rate-limiting step for this process and not the net ΔG.

Voltage and pH govern Nramp metal transport kinetics

Nramp metal transport occurs through a complex multi-step mechanism, and external factors such as transmembrane voltage and pH greatly influence the efficiency of that process. In their seminal study with rat NRAMP2, Gunshin and colleagues compared Fe^{2+}-evoked currents in oocytes across voltages from 0 to −150 mV at external pH ranging from 5.5 to 7.0. Only negligible currents were observed when ΔΨ = 0, with currents increasing as ΔΨ grew more negative [17]. In addition, a lower external pH accelerated transport across all tested ΔΨ's [17]. These findings implied that the twin variables of pH and ΔΨ govern metal transport kinetics in Nramps. Chen and colleagues reproduced the strong voltage-dependence finding using radioactive metal substrate, thus demonstrating that the larger magnitude currents at more negative ΔΨ indeed corresponded to greater metal transport [74]. Rat NRAMP2 also showed an analogous voltage dependence for Mn^{2+}- and Zn^{2+}-evoked currents, demonstrating these were general properties of Nramp metal transport [154]. Numerous later studies reproduced the findings that negative ΔΨ and/or lower external pH accelerated metal transport and/or metal-stimulated inward currents for rat NRAMP2 [116, 163, 165, 180] and extended these observations to the highly similar mouse NRAMP2 [144, 156, 190] and human NRAMP2 [88, 109, 161, 162, 164, 191]. Interestingly, despite large fluctuations in mammalian NRAMP2 transport rates (and thus k_{cat}), the K_m remained relatively constant across varied voltages [17, 109, 157] and pHs [109, 180], suggesting that those variables do not drastically affect metal binding for these homologs but instead control a separate rate-limiting step in the transport process.

Results with mammalian NRAMP1 homologs are more inconsistent. In mouse macrophages, NRAMP1-dependent Mn^{2+} efflux required the endogenous acidic-inside pH gradient across the phagosomal membrane [90]. For mouse NRAMP1 heterologously expressed in mammalian cells, one study showed greater activity at higher external pH [156] but another demonstrated the opposite [88], while in both cases mouse NRAMP1 had a much lower maximum transport activity than mouse NRAMP2. Another study with mouse NRAMP1 and human NRAMP1 in oocytes found voltage-dependent metal-elicited inward currents at neutral and slightly basic—but not acidic—external pH [94]. Radioactive Zn^{2+} uptake was also significantly higher at basic pH [94]. Lastly, a study showed that vertebrate NRAMP1s could not provide high-affinity metal import but instead conferred heavy-metal tolerance in yeast (the opposite results as seen with NRAMP2 transporters) [95], further underscoring possible mechanistic differences between the paralogs. Additional functional studies are needed to reconcile the existing data and/or explain this potential divergence within vertebrate Nramps.

Experiments with yeast Smf1p in oocytes showed a voltage-dependence trend of Fe^{2+}-associated currents similar to those seen in mammalian NRAMP2 [74], while lower pH and more negative ΔΨ each also accelerated radioactive Mn^{2+} uptake [169]. Acidic pH of the

medium also stimulated greater metal uptake by *C. neoformans* NRAMP1 [73] and *D. discoideum* NRAMP1 [170]. Acidic external pH stimulated metal transport in several prokaryotic Nramp homologs, including *S.* Typhimurium Nramp [37], *Mycobacterium tuberculosis* Nramp [34], EcoleNramp [140], and EcoliNramp [37, 38, 145]. For EcoliNramp, pH did not greatly affect the K_m for Mn^{2+} [37], but did perturb the K_m for Cd^{2+} in a separate study [142].

In proteoliposome assays using metal-sensitive dyes, DraNramp exhibited similar trends of voltage and pH dependence as seen in well-studied eukaryotic homologs, although with a couple notable differences. For one, the threshold $\Delta\Psi$ required for observable metal transport varied significantly based on metal elemental identity, with weak (high K_m) substrates such as Co^{2+} not transported until significantly negative $\Delta\Psi$ (−80 mV), while strong (low K_m) substrates like as Cd^{2+} were transported even at $\Delta\Psi > 0$ [132]. Acidic external pH also accelerated metal transport, but pH had a larger magnitude effect on Mn^{2+} than Cd^{2+} transport [132]. Additionally, in contrast to mammalian NRAMP2, $\Delta\Psi$ and pH dictated not only the V_{max}, but also the K_m—for example, lowering $\Delta\Psi$ from −50 to −150 mV decreased the K_m for Mn^{2+} >300 fold—suggesting that these variables could affect both metal binding and the rate-limiting step [132]. Comparably rigorous studies with other prokaryotic and eukaryotic homologs could help elucidate the basis for any potential mechanistic divergences in the Nramp family.

In general, metal import by Nramps requires a negative-inside membrane potential, which provides both a thermodynamic and kinetic impetus for metal entry. In addition, acidic external pH typically also stimulates metal uptake—as would be expected for a proton/metal symporter—although the ideal pH may vary by homolog. Ultimately, the strong voltage and pH dependence that are hallmarks of the Nramp family may be mechanistic adaptations to accelerate metal uptake under physiological conditions while discouraging any deleterious back-transport of cytosolic metal reserves. As backward transport would typically have to overcome a physiological $\Delta\Psi > 0$ and unfavorable ΔpH, these properties may therefore help erect an insurmountable kinetic barrier to prevent the loss of essential micronutrients.

Proton transport is a general feature of the Nramp family

Along with demonstrating its function as a metal transporter, Gunshin and colleagues documented that rat NRAMP2 also transports protons in transfected oocytes. Applying a lower external pH and a negative-inside membrane potential led to inward currents (indicating cation entry), while a simultaneous observed drop in intracellular pH confirmed that H^+ movement (proton uniport) contributed to the current. Adding Fe^{2+} enhanced both the inward current and intracellular acidification, suggesting proton-metal cotransport [17]. Concurrently measuring inward currents and radioactive Fe^{2+} entry at multiple membrane potentials, Chen and colleagues then calculated that a highly variable fraction of the total charge movement could be attributed to divalent cation transport. Therefore, if H^+ movement contributed all the excess charge, the H^+:Fe^{2+} transport stoichiometry was not fixed; instead it increased from ~1:1 at +10 mV to >10:1 at −50 mV and >20:1 at −80 mV [74]. Lowering the external pH further skewed the cotransport stoichiometry [163]. Similar results were also observed with Mn^{2+}, Co^{2+}, and Zn^{2+} in later studies [163, 169]. These findings indicate

relatively loose coupling between metal and proton cosubstrates: rat NRAMP2 deviates from the canonical model of secondary transport in which protein structure enforces a precise cotransport stoichiometry [192]. Analogous currents attributable to proton uniport and proton-metal symport were obtained with human NRAMP2 [109, 157, 168] and mouse NRAMP2 [144], although without explicitly demonstrating H^+ movement. Expression of human NRAMP2 did lead to intracellular acidification upon Fe^{2+} addition in a separate study [158], providing further evidence that mammalian NRAMP2 transports protons. Mackenzie and colleagues noted a similar temperature dependence for H^+ uniport and Fe^{2+}/H^+ cotransport currents, suggesting a similar activation energy barrier, perhaps due to similar-magnitude conformational changes required for both processes [109]. However, the reason for the huge variability in cotransport stoichiometry seen for mammalian NRAMP2 [74] remains undetermined. Perhaps metal-bound NRAMP2 passes through a state in which rapid H^+ shuttling can occur, at a rate determined by environmental ΔpH and $\Delta\Psi$, before the conformational change process fully seals the external vestibule.

Nramps from other eukaryotic species also transport protons, although some homologs have additional peculiarities. Similar to mammalian NRAMP2, studies in oocytes with yeast Smf1p demonstrated proton uniport currents at low external pH and larger magnitude proton-metal symport currents [74, 169]. However, Chen and colleagues reported a striking mechanistic difference compared to mammalian homologs: Smf1p and Smf2p mediated significant inward cationic currents in the presence of Na^+, Li^+, Rb^+, or K^+—but not the larger organocation choline. These cation fluxes were antagonistic to metal transport, as added Fe^{2+} somewhat inhibited these currents and the presence of Na^+ reduced Fe^{2+} uptake [74]. Smf1p also enabled significant uptake of radioactive Ca^{2+}—typically not a substrate metal for Nramps, as described above—perhaps also through a similar non-specific cation pathway [74]. As these unorthodox behaviors were not seen in parallel experiments with rat NRAMP2 [74], it remains to be determined whether yeast Nramps are outliers in exhibiting this cation leak, what is the mechanism for this charge movement, and why this feature evolved. Another possible deviation from expected Nramp proton transport behavior was seen in *D. discoideum* NRAMP1 [170]. At acidic pH, added metal stimulated inward currents but no H^+ uniport currents were detected, and instead larger magnitude basal currents were observed at slightly basic conditions, which addition of metal partially repressed [170]. In studies with human NRAMP1 and mouse NRAMP1, which may have an opposite pH dependence of transport rate as mammalian NRAMP2 [156], adding external Zn^{2+} coincided with an intracellular pH rise [94], suggesting possible metal/proton antiport behavior.

Several studies with prokaryotic Nramps have confirmed similar proton-transport behavior to the canonical mammalian homologs. In *E. coli* overexpressing EcoliNramp, adding Cd^{2+} at a low external pH stimulated intracellular acidification as monitored using a pH-sensitive GFP-derivative [137, 142, 177], although, surprisingly, adding Nramp substrates Mn^{2+}, Fe^{2+}, and Co^{2+} did not similarly perturb the intracellular pH [177]. Additionally, providing Mn^{2+} to *E. coli* prompted an EcoliNramp-dependent increase in external pH as measured with a cell impermeable fluorescent dye [181], while adding a protonophore eliminated Mn^{2+} transport attributed to EcoliNramp [38]. For EcoleNramp in proteoliposomes loaded

with a pH-sensing dye, Ehrnstorfer and colleagues demonstrated a basal voltage-driven H^+ movement and a concentration-dependent Mn^{2+}-enhancement of this H^+ transport [140].

With DraNramp, we documented analogous voltage-driven, protein-dependent H^+ transport using a pH-sensing dye in proteoliposomes [132, 136]. However, under conditions in which metal cations were also transported (confirmed using metal-binding dyes), Mn^{2+}, Fe^{2+}, and Co^{2+} stimulated additional H^+ entry, while Zn^{2+} and Cd^{2+} did not, with Cd^{2+} notably reducing H^+ transport below the no-metal baseline rate [132]. From comparing initial rates, approximate cotransport stoichiometries of 1 H^+:1 Mn^{2+} and 0 H^+:1 Cd^{2+} were calculated, with the implication that while Mn^{2+} (and Fe^{2+} and Co^{2+}) undergo proton-metal symport, Cd^{2+} (and Zn^{2+}) instead undergo metal uniport. Interestingly, pH affected the kinetics of both Cd^{2+} and Mn^{2+} transport, with lower pH increasing the rate [132], demonstrating protons have multiple roles in the Nramp transport process. Whether DraNramp's metal-specific proton cotransport behavior is a general feature of the Nramp family or a specific adaptation to reduce Cd^{2+} overaccumulation in a homolog from a particularly Mn^{2+}-hungry species [193] remains undetermined.

To summarize, both prokaryotic and eukaryotic Nramp transporters also conduct protons from outside to inside down their electrochemical gradient in addition to transition metal substrates, which likely helps power potentially thermodynamically uphill metal movement. This proton transport occurs in the absence (proton "uniport") or presence of metal substrate (proton-metal "symport"). Thus, unlike in canonical symporters, proton and metal substrates are not tightly coupled, and proton:metal stoichiometry can vary depending on transmembrane voltage, pH gradients, and metal elemental identity.

The metal-binding aspartate is also important for proton transport

While most x-ray crystallographic experiments do not allow direct visualization of protons, the available Nramp structures, supplemented with sequence analysis, provide a good starting point to understand Nramp proton binding and transport. Intuitively, proton transport requires protonatable residue(s). The Nramp family features a conserved core network of protonatable residues not found in structurally related LeuT-fold outgroups [194], including members known to also transport protons [195–198]. This network's opportune location for such a purpose is apparent in the available structures of ScaNramp [139], EcoleNramp [140], and DraNramp [134, 136] (Figure 6). In DraNramp, the key triad of D56 on TM1, H232 on TM6b, and E134 on TM3 connect the metal-binding site to a pair of conserved salt bridges that link TM3 and TM9, with D131-R353 in the middle of the membrane and R352-E124 closer to the cytosol (Figure 6(a)) [136]. A bevy of conserved polar amino acids on TMs 3, 4, 8, and 9 flank these residues to form a 20 Å hydrophilic pathway for protons to transit, with the analogous networks in ScaNramp and EcoleNramp also including a third TM9 arginine and an extra aspartate on TM4 (Figure 6(a)) [139, 140]. Mutational studies illustrated the importance of members of this hydrophilic network to metal transport in DraNramp [132, 135], EcoliNramp [142, 145, 177, 178], EcoleNramp [140], human NRAMP2 [26, 157], mouse NRAMP2 [124, 144, 183], and rat NRAMP2 [180]. Underscoring the network's importance, some NRAMP2 mutations to this network or its vicinity cause anemia in mammals, including R416C (M357, the likely functional equivalent

of R353) in humans, and G185R (G153) in mice and rats (Figure 2(c)) [26, 124, 144]. A list of key residues in this network and a summary of reported mutagenesis effects on Nramp's proton transport and proton-metal coupling properties are provided in Table 5.

The essential metal-binding site aspartate (D56) is also the most likely initial protonation site (Figure 6(b)). Consistent with the expected behavior of acidic residues located at a protein's core [199], D56's predicted pK_a shifts upward, to 6.7 in DraNramp [136] and 6.8 in ScaNramp [139, 157], putting it in the optimal range for rapid protonation/deprotonation at physiological pH. As expected, the mutations D56A and D56N eliminated both H^+ uniport and Mn^{2+}/H^+ symport in DraNramp [132, 136], while analogous mutations in EcoleNramp in proteoliposomes [140] and EcoliNramp *in vivo* [181] similarly disrupted Mn^{2+}-stimulated H^+ movement. Protonation of D56 may optimize the binding site for incoming metal through enabling it to donate a hydrogen bond to the adjacent metal-binding N59, thus properly orienting its carbonyl oxygen to coordinate incoming metal. In DraNramp, N59A retained WT-like H^+ uniport [132, 136] but eliminated Mn^{2+}/H^+ symport [132], as was also seen in the analogous EcoleNramp mutant [140]. The nearby metal-binding site methionine may also play a crucial role in enforcing metal-proton coupling. While the DraNramp M230A mutant performed both H^+ uniport [132, 136] and Mn^{2+}/H^+ symport [132], acidic pH no longer accelerated Mn^{2+} uptake, and Cd^{2+} appeared to also undergo H^+ symport rather than the uniport seen with WT [132]. In EcoleNramp in contrast, the analogous M-to-A mutants surprisingly showed no Mn^{2+}-stimulation of H^+ transport despite retaining measurable Mn^{2+}-transport ability [140]. Thus, while D56 is likely the essential proton-transfer point, the entire conserved metal-binding site enables non-canonical proton-metal coupling in Nramps. In addition, for Cd^{2+} and Zn^{2+}, which often prefer different coordination geometries than other Nramp metal substrates, a monodentate interaction with D56 (which would allow retention of the proton) could explain the lack of H^+ cotransport stimulation seen for transport of these cations by DraNramp [132].

Two highly conserved histidines on TM6b are key to coordinating conformational cycle

Below the metal-binding site on TM6b, two highly conserved histidine are essential for WT-like metal transport in all tested homologs. The first, H232, is located just beneath M230, while the second, H237 is found further down the helix along the cytosolic metal-release pathway (Figure 6). In EcoliNramp, mutations of either histidine impaired Mn^{2+} uptake, with glutamine replacements preserving the most function [145]. Similarly, all tested mutations to either histidine besides H232Q sharply reduced or eliminated Co^{2+} and Mn^{2+} transport in *E. coli* expressing DraNramp [135]. Analogous histidine mutations reduced metal transport in mammalian cells transfected with mouse NRAMP2 [183] and reduced Fe^{2+} uptake in oocytes expressing rat NRAMP2 [180], with arginine replacements consistently inactive for all species.

Mutations to H232 in DraNramp perturbed the protein's conformational cycling as assessed using a single cysteine reporter, as H232A hardly sampled the outward-open state, while the bulky replacement H232R yielded an inward-locked transporter [135]. Intriguingly, for the

H232F mutation, outward-reporter labeling plateaued at 50% of the protein population [135], suggesting a static equilibrium due to a significant rise in the activation energy barrier to bulk conformational change and providing further evidence of TM6b's essential role in that process. In proteoliposome studies, H232Q preserved significant metal transport but prevented all H^+ transport and eliminated any pH dependence of the Mn^{2+} transport rate [132]. In DraNramp, H232 therefore likely both stabilizes the proton transfer from D56 to D131 (Figure 6(b); as described below) and serves as a pivot point for the bulk conformational change needed for metal transport to occur. The H234A mutation of the equivalent residue in EcoleNramp had the same effects on metal and proton transport, leading to the proposal that this histidine is the likely proton-binding site [140]. However, its location in the protein core should disfavor it bearing a formal charge, as evidenced by the residue's estimated pK_a of 3.6 in DraNramp [136] and 4.7 in ScaNramp [139, 157]. Interestingly, H234A EcoleNramp was crystallized in the outward-open state, perhaps suggesting a less important role in conformational change for that homolog [140]. Results with H232 variants differed for mammalian Nramp homologs. In mouse NRAMP2, the analogous H267A and H267C mutants, while less active compared to WT, displayed significant pH dependence of metal transport as measured using fluorescent dyes, with higher activity at acidic pH [183]. Similarly, in rat NRAMP2 expressed in oocytes, the H267A mutation reduced overall activity, but preserved WT-like pH dependence of radioactive metal uptake and intracellular acidification upon Fe^{2+} addition, suggesting an intact H^+ transport pathway [180].

The second key histidine, H237, was also essential to proper conformational cycling in DraNramp, as all tested replacements yield transporters incapable of significantly sampling the outward-open state [135]. In proteoliposomes, the H237Q mutant exhibited no proton transport and only slight, but pH-sensitive, metal transport. In mouse NRAMP2, H272A and H272C mutations had similar effect as H267 mutants, with reduced, but still pH dependent, Fe^{2+} transport [183]. In contrast, the H272A mutation in rat NRAMP2 appeared to fully decouple H^+ and metal transport, such that the cosubstrates even competed with rather than stimulated each other [180]. This mutant displayed pH-independent radioactive Fe^{2+} transport, at an overall reduced level compared to WT. In addition, H272A showed much larger magnitude H^+ currents than WT leading to rapid intracellular acidification, and these currents were partially inhibited rather than stimulated by Fe^{2+} addition. These two key histidines therefore appear to contribute in some manner to conformational change and metal-proton coupling—though likely not through direct protonation/deprotonation—in all Nramp homologs, but their precise roles may vary by species.

Conserved charged residues are important for proton transport and proton-metal coupling

Three highly conserved acidic residues line one face of TM3 between the metal-binding site and the cytosol, E134, D131, and E124 (Figure 6). As the structural link between the salt-bridge network and D56, E134 is intricately involved in proton-metal coupling. The mutations E134A and E134Q nearly eliminated H^+ transport in DraNramp and greatly reduced the pH dependence of Mn^{2+} transport [132, 136]. The analogous mutations

drastically reduced Mn^{2+} uptake [178] and Mn^{2+}-stimulated H^+ transport [181] in EcoliNramp. In contrast, while E129A in EcoleNramp appeared to decouple metal and proton transport—eliminating the pH dependence of Mn^{2+} transport while drastically increasing the rate of H^+ uniport—E129Q behaved nearly identically to WT. The latter result, along with a predicted $pK_a > 10$ in DraNramp [136] and ScaNramp [139, 157], argued against that glutamate being a key proton transfer point [140]. In human NRAMP2, the analogous E164A mutant retained some pH-dependent metal transport but nearly eliminated metal-evoked currents—perhaps due to a lack of H^+ cotransport—and pre-steady state currents attributed to charge rearrangements in the apo transporter [157]. An E164D mutant deviated less from WT, with significant H^+ uniport and shifted pH dependence of Fe^{2+} transport [157], further demonstrating the ability of perturbations at this crucial position to disrupt proton-metal coupling.

Mutations to the adjacent TM3 aspartate, D131A and D131N in DraNramp, eliminated all H + transport while reducing pH dependence of Mn^{2+} transport [132]. The analogous D109N mutation greatly reduced Mn^{2+} uptake [178] and eliminated Mn^{2+}-stimulated intracellular acidification in *E. coli* expressing EcoliNramp [181]. This residue has a predicted pK_a of 4.9 in DraNramp [136] and ScaNramp [139, 157], suggesting its amenability to protonation, especially as the most obvious proton acceptor candidate upon metal substrate binding to D56 (which is predicted to drastically downshift its pK_a and thus prompt deprotonation). Mutations to the TM3 glutamate proximal to the cytosol, E124, decoupled proton and metal transport in DraNramp. Compared to WT, E124A and E124Q reduced the pH dependence of the Mn^{2+} transport rate while increasing H^+ uniport, which was then partially inhibited rather than stimulated by Mn^{2+} addition [132]. In EcoliNramp the analogous E102N also greatly reduced Mn^{2+} transport [178] and Mn^{2+}-stimulated H^+ entry [181].

Two TM9 arginines form salt bridges with TM3 acidic residues (Figure 6). Mutations of either arginine to alanine in DraNramp—R352A or R353A—also perturbed proton-metal coupling, reducing the pH dependence of Mn^{2+} transport rate and increasing H^+ uniport [132, 136]. In addition, Mn^{2+} and Cd^{2+} both stimulated H^+ cotransport for R352A but inhibited H^+ entry for R353A [132]. Intriguingly, the F196I (L164) mutation at the bottom of TM4 adjacent to the lower salt-bridge pair in rat NRAMP2 preserved WT-like Fe^{2+} uptake but greatly reduced total inward current, suggesting that it decreased the accompanying H^+ entry [163]. Future in-depth studies testing wider panels of mutants in mammalian NRAMP2 would help to either confirm conserved roles for the salt-bridge residues in the transport process or else begin to elucidate potential mechanistic differences between homologs. In summary, while D56 and D131, assisted by H232 and E134, appear to form the essential core of the proton transfer pathway, the surrounding metal-binding site and the extended salt-bridge network residues all contribute to enforcing proton-metal coupling.

The conserved charged residues also influence voltage dependence of metal transport

As detailed above, Nramp metal transport is influenced by the membrane potential. Mn^{2+} transport by DraNramp is highly voltage dependent, ranging from no measurable transport at $\Delta\Psi = 0$ mV to near-maximal transport at $\Delta\Psi = -100$ mV [132]. Mutations to each of E124, D131, E134, R352, and R353 greatly reduced the physiological voltage dependence of metal transport rate in DraNramp, such that significant Mn^{2+} transport still occurred at $\Delta\Psi = 0$ mV, while mutations to N59, M230, H232, and H237 preserved WT-like behavior [132]. In addition, in a proteoliposome experiment in which outside-out transporters were selectively disabled using membrane-impermeable cysteine modifiers, leaving only inside-out transporters active, WT-like protein showed little metal transport activity but the variants D131N, E134A, and R352A all retained significant activity [132]. Thus, disruptions to the conserved Nramp salt-bridge network which perturbed the strong voltage dependence also reduced or eliminated directional bias in transport. In a cellular context, this would correspond to a much larger efflux of metals from the cytosol, clearly a deleterious property for a metal importer.

Emerging mechanistic model for Nramp transporters

In the last several sections, we described how a pathway for proton transport in Nramps uses a conserved network of hydrophilic residues that originates from the metal-binding site and extends 20 Å to the cytosol between TMs 3, 4, 8, and 9. Furthermore, proton shuttling likely relies on two strategically located aspartates (D56 and D131) that sequentially protonate/deprotonate. Several additional surrounding charged/protonatable residues that participate in a series of salt-bridge interactions enforce this non-canonical metal-proton coupling, impart the observed strong voltage dependence of metal transport rate, and may serve to prevent deleterious metal back-transport.

From all the results discussed above, we proposed that Nramp proton-metal cotransport occurs via the following general mechanism (Figure 6(c)). First, D56 is protonated, which orients the binding site for metal binding and thus imparts some of the observed pH dependence of Nramp metal transport. Incoming metal substrate displaces the proton from D56, causing proton transfer past E134 and H232 to D131, leading ultimately to proton dissociation to the cytosol through the TM3-4-8-9 salt-bridge network. Metal binding and the concomitant proton transfer trigger the bulk conformational change, with the outside vestibule closing and the cytosolic vestibule opening, thus facilitating eventual metal release. This would also serve to mechanistically couple the two co-substrates. Proton uniport also uses the salt-bridge network without requiring large-scale conformational rearrangement.

Overall, functional adaptations of Nramps compared to structural homologs like LeuT—most notably the salt-bridge network that forms a separate pathway for proton release—appear to encode the ability for non-canonical cosubstrate coupling. Unlike LeuT and other sodium-driven symporters of small organic molecules, the Nramp cosubstrates' binding is not fully synergistic, and the two cations likely do not coexist in the binding site through an arrangement that would enforce a tight stoichiometry [6, 14]. Instead, the structure of

Nramps may facilitate an alternative coupling mechanism in which proton movement through the salt-bridge network helps shift the protein's conformational landscape to favor the transition to the inward-open metal release state. Therefore, most—but not all—metal substrates require H^+ cotransport, and H^+ uniport occurs without added metal (Figure 7). Although this arrangement is energetically wasteful by depleting the transmembrane proton gradient, it may have evolved to prevent electrostatic repulsion between cation cosubstrates and may serve to make the metal-transport step kinetically irreversible. That a simple hydrophobic substitution along the proton-transport route could apparently tighten the coupling between the two cosubstrates without impairing metal transport [163] raises the intriguing question of whether these loosely coupled proton fluxes serve a designed functional purpose rather than merely being a tolerated bug of the transporter. Indeed, mutations to the conserved salt-bridge network that preserved metal transport but completely eliminated proton cotransport also increased the rate of metal export [132]. Thus, the non-canonical coupling and strong voltage dependence of metal transport rate of Nramps, imparted by a unique salt-bridge network, may encourage unidirectional substrate movement under physiological conditions. This property ultimately represents a potential functional advantage over a traditional, fully reversible/bidirectional symporter.

Conclusions and outlook

Since the discovery of the Nramp family and the initial characterization of mammalian and yeast homologs as transition metal transport proteins in the mid-1990s, subsequent work has illustrated the widespread distribution of these proteins throughout the tree of life and their roles in numerous biological contexts. Over two decades' worth of functional studies with several model Nramp homologs support a generally conserved mechanism for metal transport that involves proton cotransport and a kinetic role for voltage, as well as a propensity for uncoupled proton flux. More recently, multiple crystal structures for three prokaryotic homologs have revealed how Nramp uses a common secondary-transporter fold with unique structural adaptations to selectively bind transition metals, undergo alternating-access to translocate metal cargo, and shuttle protons down a parallel conserved exit pathway to separate the like-charge cosubstrates during the transport process.

Despite the wealth of structural information and functional data, many additional questions about the Nramp molecular mechanism remain unanswered, as recently highlighted by Rudnick [200]. First, are transition metal ions and protons indeed thermodynamically coupled, such that a favorable gradient of either cosubstrate can drive uphill transport of the other? Proteoliposome experiments using pH gradients and radioactive metal ions could begin to provide an answer to this question. Second, the precise mechanism through which the pronounced kinetic voltage dependence of Nramps [17, 132] is enforced remains murky, and it could involve rearrangements of any of the numerous conserved charged residues or the movement of the charged substrates themselves. As membrane potential magnitudes vary significantly depending on biological context, voltage may impact different steps of the transport process for different homologs, as suggested by its differential effects on K_m values for bacterial and mammalian homologs [109, 132]. Future molecular dynamics simulations or perhaps *in crystallo* voltage application [201] could help provide the missing details. Third, is the bulk conformational change from outward-open to inward-open states

initiated by substrate binding in Nramps, as the incomplete metal-coordination sphere seen in outward-open DraNramp might suggest? Sophisticated *in vitro* experiments using pairs of reporters at key positions seen to rearrange during the conformational change process for Förster resonance energy transfer (FRET) or double electron-electron resonance (DEER) could begin to unravel how substrate(s) binding affects the conformational landscape of an Nramp transporter. Fourth, while proton uniport occurs through the outward-open state [136] and the same key salt-bridge network residues are required for both proton uniport and metal-stimulated proton cotransport [132], the precise route taken by protons remains undetermined, and could involve additional protonation states. Moreover, how metal cotransport and the associated conformational change affects this process remains unknown, and future experiments and molecular dynamics simulations are necessary to elucidate additional details about the proton transport route and the precise order of the key molecular events required for proton-metal cotransport (proton binding, metal binding, proton transfer, conformational change, metal release, proton release).

Although metal transport in many disparate Nramp homologs likely occurs through a common general mechanism, potential discrepancies in the details between homologs require further investigation. First, regarding metal selectivity, bacterial Nramps greatly favor Mn^{2+} transport over other similar metals [132], while eukaryotic homologs transported most metal substrates with similar apparent affinities [161]. As the TM1 and TM6 metal-binding residues are conserved across Nramp clades, the structural basis for this Mn^{2+} specialization is not obvious and may involve more subtle differences at positions outside the inner coordination sphere that additional high-resolution structures with a range of metal substrates or rigorous mutagenesis studies may help unravel. Techniques such as electron paramagnetic resonance (EPR) or X-ray absorption fine structure (XAFS) could also elucidate the electronic properties of the metal and its interactions with the surrounding metal-coordinating amino acid and water ligands during the transport process. Second, the high variability in cotransport stoichiometries for mammalian NRAMP2—with up to 20 protons for each transported metal ion [74]—may differ in bacterial homologs, as DraNramp maintained close to a 1:1 H^+:M^{2+} cotransport ratio [132]. Furthermore, the mechanistic basis for how mammalian Nramps facilitate these large proton fluxes at saturating metal concentrations remains unknown. It also remains undetermined whether the metal-specific proton cotransport seen with DraNramp is a general feature or an adaptation of a smaller branch of the Nramp family. Future investigations that directly track protonation-deprotonation events spectroscopically *in vitro*, such as nuclear magnetic resonance (NMR) or Fourier transform infrared (FTIR) spectroscopy—as well as MD simulations to model protein behavior under various conditions—would help answer these questions. Third, the high permeability of yeast Smf1p to Na^+, Ca^{2+}, and similar cations—in a competitive manner with H^+ and transition metal passage [74]—lacks a mechanistic explanation. While fungal Nramps have significantly diverged from both prokaryotic and other eukaryotic homologs [20], they retain the same metal-binding site and proton-transport pathway residues. In-depth evolutionary analyses and mutagenesis studies may elucidate the basis for this non-canonical feature. Last, the mechanism and functional role of vertebrate NRAMP1 transporters remains disputed, with evidence for H^+/M^{2+} symport supporting a role in metal withholding [88], while conflicting results suggesting H^+/M^{2+} antiport led to speculation of

intentional bombardment of pathogens with redox-active metal cations [94]. In addition, the recent report that mammalian NRAMP1 induces Mg^{2+} starvation in intracellular pathogens suggests another potential functional divergence for this homolog [91]. While evolutionary arguments currently favor a common transition metal-extraction symport role [33], rigorous *in vitro* studies are needed to firmly establish NRAMP1's transport mechanism and substrate selectivity profile.

Throughout evolutionary history organisms successfully adapted Nramp homologs to provide metal transport in myriad biological contexts. Thanks to years of functional studies and more recent structural advances, Nramps are now one of the few secondary transport protein families whose mechanism we are beginning to understand at an atomic level. As detailed above, this mechanism deviates significantly from generally accepted transport models for structural homologs such as LeuT in many ways: distinct conformational rearrangements to achieve alternating access, separate transport pathways for metal and proton cosubstrates, asymmetric coupling leading to variable cotransport stoichiometries, overarching importance of voltage to both the kinetics and thermodynamics of transport, and directionally biased substrate movement. Nramps may ultimately prove to be valuable model systems for understanding non-canonical secondary active transport behavior more broadly, and many of its apparently quirky properties may turn out to be more widespread evolutionarily, such as the substrate-specific cotransport stoichiometries seen in other transporters (e.g., [202, 203]). Further mechanistic study of Nramp family members as well as other distantly related and unrelated transporters will continue to enhance our understanding of the fundamental principles of membrane transport.

Acknowledgements

We would like to thank Lukas Bane, Wilhelm Weihofen, Christina Zimanyi, Shamayeeta Ray, Anne McCabe, Jack Nicoludis, Brandon Lee, Casey Zhang, Ben Barnett, Jenifer Brown, Sriram Srikant, Abhishek Singharoy, and other Gaudet lab members and collaborators who have contributed to Nramp-related research and discussions over the years. This work was funded by NIH grant R01GM120996 (to R.G.).

References

[1]. Posey JE, Gherardini FC. Lack of a role for iron in the Lyme disease pathogen. Science. 2000;288:1651–3. [PubMed: 10834845]

[2]. Cassat JE, Skaar EP. Iron in infection and immunity. Cell Host Microbe. 2013;13:509–19. [PubMed: 23684303]

[3]. Archibald F. *Lactobacillus plantarum*, an organism not requiring iron. FEMS Microbiology Letters. 1983;19:29–32.

[4]. Kolber ZS, Barber RT, Coale KH, Fitzwateri SE, Greene RM, Johnson KS, et al. Iron limitation of phytoplankton photosynthesis in the equatorial Pacific Ocean. Nature. 1994;371:145–9.

[5]. Boudker O, Verdon G. Structural perspectives on secondary active transporters. Trends Pharmacol Sci. 2010;31:418–26. [PubMed: 20655602]

[6]. Rudnick G. How do transporters couple solute movements? Mol Membr Biol. 2013;30:355–9. [PubMed: 24147977]

[7]. Shi Y. Common folds and transport mechanisms of secondary active transporters. Annu Rev Biophys. 2013;42:51–72. [PubMed: 23654302]

[8]. Forrest LR, Kramer R, Ziegler C. The structural basis of secondary active transport mechanisms. Biochim Biophys Acta. 2011;1807:167–88. [PubMed: 21029721]

[9]. Gadsby DC. Ion channels versus ion pumps: the principal difference, in principle. Nat Rev Mol Cell Biol. 2009;10:344–52. [PubMed: 19339978]

[10]. Shilton BH. Active transporters as enzymes: an energetic framework applied to major facilitator superfamily and ABC importer systems. Biochem J. 2015;467:193–9. [PubMed: 25837849]

[11]. Perez C, Ziegler C. Mechanistic aspects of sodium-binding sites in LeuT-like fold symporters. Biol Chem. 2013;394:641–8. [PubMed: 23362203]

[12]. West IC. Energy coupling in secondary active transport. Biochim Biophys Acta. 1980;604:91–126. [PubMed: 6248113]

[13]. Henderson RK, Fendler K, Poolman B. Coupling efficiency of secondary active transporters. Curr Opin Biotechnol. 2019;58:62–71. [PubMed: 30502621]

[14]. LeVine MV, Cuendet MA, Khelashvili G, Weinstein H. Allosteric Mechanisms of Molecular Machines at the Membrane: Transport by Sodium-Coupled Symporters. Chem Rev. 2016;116:6552–87. [PubMed: 26892914]

[15]. Jardetzky O. Simple allosteric model for membrane pumps. Nature. 1966;211:969–70. [PubMed: 5968307]

[16]. Cellier M, Prive G, Belouchi A, Kwan T, Rodrigues V, Chia W, et al. Nramp defines a family of membrane proteins. Proc Natl Acad Sci U S A. 1995;92:10089–93. [PubMed: 7479731]

[17]. Gunshin H, Mackenzie B, Berger UV, Gunshin Y, Romero MF, Boron WF, et al. Cloning and characterization of a mammalian proton-coupled metal-ion transporter. Nature. 1997;388:482–8. [PubMed: 9242408]

[18]. Supek F, Supekova L, Nelson H, Nelson N. A yeast manganese transporter related to the macrophage protein involved in conferring resistance to mycobacteria. Proc Natl Acad Sci U S A. 1996;93:5105–10. [PubMed: 8643535]

[19]. Forbes JR, Gros P. Divalent-metal transport by NRAMP proteins at the interface of host-pathogen interactions. Trends in microbiology. 2001;9:397–403. [PubMed: 11514223]

[20]. Cellier MF. Nramp: from sequence to structure and mechanism of divalent metal import. Curr Top Membr. 2012;69:249–93. [PubMed: 23046654]

[21]. Mackenzie B, Hediger MA. SLC11 family of H^+-coupled metal-ion transporters NRAMP1 and DMT1. Pflugers Arch. 2004;447:571–9. [PubMed: 14530973]

[22]. Li X, Yang Y, Zhou F, Zhang Y, Lu H, Jin Q, et al. SLC11A1 (NRAMP1) polymorphisms and tuberculosis susceptibility: updated systematic review and meta-analysis. PLoS One. 2011;6:e15831. [PubMed: 21283567]

[23]. Wessling-Resnick M. Nramp1 and Other Transporters Involved in Metal Withholding during Infection. J Biol Chem. 2015;290:18984–90. [PubMed: 26055722]

[24]. Bardou-Jacquet E, Island ML, Jouanolle AM, Detivaud L, Fatih N, Ropert M, et al. A novel N491S mutation in the human SLC11A2 gene impairs protein trafficking and in association with the G212V mutation leads to microcytic anemia and liver iron overload. Blood Cells Mol Dis. 2011;47:243–8. [PubMed: 21871825]

[25]. Beaumont C, Delaunay J, Hetet G, Grandchamp B, de Montalembert M, Tchernia G. Two new human DMT1 gene mutations in a patient with microcytic anemia, low ferritinemia, and liver iron overload. Blood. 2006;107:4168–70. [PubMed: 16439678]

[26]. Lam-Yuk-Tseung S, Camaschella C, Iolascon A, Gros P. A novel R416C mutation in human DMT1 (SLC11A2) displays pleiotropic effects on function and causes microcytic anemia and hepatic iron overload. Blood Cells Mol Dis. 2006;36:347–54. [PubMed: 16584902]

[27]. Iolascon A, d'Apolito M, Servedio V, Cimmino F, Piga A, Camaschella C. Microcytic anemia and hepatic iron overload in a child with compound heterozygous mutations in DMT1 (SCL11A2). Blood. 2006;107:349–54. [PubMed: 16160008]

[28]. Yamashita A, Singh SK, Kawate T, Jin Y, Gouaux E. Crystal structure of a bacterial homologue of Na^+/Cl^--dependent neurotransmitter transporters. Nature. 2005;437:215–23. [PubMed: 16041361]

[29]. Vastermark A, Wollwage S, Houle ME, Rio R, Saier MH Jr. Expansion of the APC superfamily of secondary carriers. Proteins. 2014;82:2797–811. [PubMed: 25043943]

[30]. Wong FH, Chen JS, Reddy V, Day JL, Shlykov MA, Wakabayashi ST, et al. The amino acid-polyamine-organocation superfamily. J Mol Microbiol Biotechnol. 2012;22:105–13. [PubMed: 22627175]

[31]. Cellier MF, Bergevin I, Boyer E, Richer E. Polyphyletic origins of bacterial Nramp transporters. Trends Genet. 2001;17:365–70. [PubMed: 11418195]

[32]. Richer E, Courville P, Bergevin I, Cellier MF. Horizontal gene transfer of "prototype" Nramp in bacteria. J Mol Evol. 2003;57:363–76. [PubMed: 14708570]

[33]. Cellier MF, Courville P, Campion C. Nramp1 phagocyte intracellular metal withdrawal defense. Microbes Infect. 2007;9:1662–70. [PubMed: 18024118]

[34]. Agranoff D, Monahan IM, Mangan JA, Butcher PD, Krishna S. *Mycobacterium tuberculosis* expresses a novel pH-dependent divalent cation transporter belonging to the Nramp family. J Exp Med. 1999;190:717–24. [PubMed: 10477555]

[35]. Hohle TH, O'Brian MR. The *mntH* gene encodes the major Mn^{2+} transporter in *Bradyrhizobium japonicum* and is regulated by manganese via the Fur protein. Mol Microbiol. 2009;72:399–409. [PubMed: 19298371]

[36]. Kehl-Fie TE, Zhang Y, Moore JL, Farrand AJ, Hood MI, Rathi S, et al. MntABC and MntH contribute to systemic *Staphylococcus aureus* infection by competing with calprotectin for nutrient manganese. Infect Immun. 2013;81:3395–405. [PubMed: 23817615]

[37]. Kehres DG, Zaharik ML, Finlay BB, Maguire ME. The NRAMP proteins of *Salmonella typhimurium* and *Escherichia coli* are selective manganese transporters involved in the response to reactive oxygen. Mol Microbiol. 2000;36:1085–100. [PubMed: 10844693]

[38]. Makui H, Roig E, Cole ST, Helmann JD, Gros P, Cellier MF. Identification of the *Escherichia coli* K-12 Nramp orthologue (MntH) as a selective divalent metal ion transporter. Mol Microbiol. 2000;35:1065–78. [PubMed: 10712688]

[39]. Shabayek S, Bauer R, Mauerer S, Mizaikoff B, Spellerberg B. A streptococcal NRAMP homologue is crucial for the survival of *Streptococcus agalactiae* under low pH conditions. Mol Microbiol. 2016;100:589–606. [PubMed: 27150893]

[40]. Shu HY, Tian BM. Function analysis of two Mn(II) ion transporter genes (DR1709 and DR2523) in *Deinococcus radiodurans*. African Journal of Biotechnology. 2010;9:2742–7.

[41]. Perry RD, Craig SK, Abney J, Bobrov AG, Kirillina O, Mier I, et al. Manganese transporters Yfe and MntH are Fur-regulated and important for the virulence of *Yersinia pestis*. Microbiology (Reading). 2012;158:804–15. [PubMed: 22222497]

[42]. Turner MS, Tan YP, Giffard PM. Inactivation of an iron transporter in Lactococcus lactis results in resistance to tellurite and oxidative stress. Appl Environ Microbiol. 2007;73:6144–9. [PubMed: 17675432]

[43]. Champion OL, Karlyshev A, Cooper IAM, Ford DC, Wren BW, Duffield M, et al. *Yersinia pseudotuberculosis* mntH functions in intracellular manganese accumulation, which is essential for virulence and survival in cells expressing functional Nramp1. Microbiology (Reading). 2011;157:1115–22. [PubMed: 21183572]

[44]. Anderson ES, Paulley JT, Gaines JM, Valderas MW, Martin DW, Menscher E, et al. The manganese transporter MntH is a critical virulence determinant for *Brucella abortus* 2308 in experimentally infected mice. Infect Immun. 2009;77:3466–74. [PubMed: 19487482]

[45]. Boyer E, Bergevin I, Malo D, Gros P, Cellier MF. Acquisition of Mn(II) in addition to Fe(II) is required for full virulence of *Salmonella enterica* serovar Typhimurium. Infect Immun. 2002;70:6032–42. [PubMed: 12379679]

[46]. Runyen-Janecky L, Dazenski E, Hawkins S, Warner L. Role and regulation of the *Shigella flexneri* sit and MntH systems. Infect Immun. 2006;74:4666–72. [PubMed: 16861654]

[47]. Zaharik ML, Cullen VL, Fung AM, Libby SJ, Kujat Choy SL, Coburn B, et al. The *Salmonella enterica* serovar typhimurium divalent cation transport systems MntH and SitABCD are essential for virulence in an Nramp1G169 murine typhoid model. Infect Immun. 2004;72:5522–5. [PubMed: 15322058]

[48]. Reeve I, Hummel D, Nelson N, Voss J. Overexpression, purification, and site-directed spin labeling of the Nramp metal transporter from *Mycobacterium leprae*. Proc Natl Acad Sci U S A. 2002;99:8608–13. [PubMed: 12077319]

[49]. Kajfasz JK, Katrak C, Ganguly T, Vargas J, Wright L, Peters ZT, et al. Manganese Uptake, Mediated by SloABC and MntH, Is Essential for the Fitness of Streptococcus mutans. mSphere. 2020;5.

[50]. Sabri M, Caza M, Proulx J, Lymberopoulos MH, Bree A, Moulin-Schouleur M, et al. Contribution of the SitABCD, MntH, and FeoB metal transporters to the virulence of avian pathogenic *Escherichia coli* O78 strain chi7122. Infect Immun. 2008;76:601–11. [PubMed: 18025097]

[51]. Helmann JD. Specificity of metal sensing: iron and manganese homeostasis in *Bacillus subtilis*. J Biol Chem. 2014;289:28112–20. [PubMed: 25160631]

[52]. Ma Z, Jacobsen FE, Giedroc DP. Coordination chemistry of bacterial metal transport and sensing. Chem Rev. 2009;109:4644–81. [PubMed: 19788177]

[53]. Patzer SI, Hantke K. Dual repression by Fe^{2+}-Fur and Mn^{2+}-MntR of the *mntH* gene, encoding an NRAMP-like Mn^{2+} transporter in *Escherichia coli*. J Bacteriol. 2001;183:4806–13. [PubMed: 11466284]

[54]. Sun H, Li M, Xu G, Chen H, Jiao J, Tian B, et al. Regulation of MntH by a dual Mn(II)- and Fe(II)-dependent transcriptional repressor (DR2539) in *Deinococcus radiodurans*. PLoS One. 2012;7:e35057. [PubMed: 22523570]

[55]. Siedler S, Rau MH, Bidstrup S, Vento JM, Aunsbjerg SD, Bosma EF, et al. Competitive Exclusion Is a Major Bioprotective Mechanism of Lactobacilli against Fungal Spoilage in Fermented Milk Products. Appl Environ Microbiol. 2020;86.

[56]. Bozzaro S, Buracco S, Peracino B. Iron metabolism and resistance to infection by invasive bacteria in the social amoeba *Dictyostelium discoideum*. Front Cell Infect Microbiol. 2013;3:50. [PubMed: 24066281]

[57]. Peracino B, Wagner C, Balest A, Balbo A, Pergolizzi B, Noegel AA, et al. Function and mechanism of action of *Dictyostelium* Nramp1 (Slc11a1) in bacterial infection. Traffic. 2006;7:22–38. [PubMed: 16445684]

[58]. Brenz Y, Ohnezeit D, Winther-Larsen HC, Hagedorn M. Nramp1 and NrampB Contribute to Resistance against *Francisella* in *Dictyostelium*. Front Cell Infect Microbiol. 2017;7:282. [PubMed: 28680861]

[59]. Thomine S, Schroeder JI. Plant Metal Transporters with Homology to Proteins of the NRAMP Family. Madame Curie Bioscience Database. 2013.

[60]. Belouchi A, Kwan T, Gros P. Cloning and characterization of the OsNramp family from *Oryza sativa*, a new family of membrane proteins possibly implicated in the transport of metal ions. Plant molecular biology. 1997;33:1085–92. [PubMed: 9154989]

[61]. Thomine S, Wang R, Ward JM, Crawford NM, Schroeder JI. Cadmium and iron transport by members of a plant metal transporter family in Arabidopsis with homology to Nramp genes. Proc Natl Acad Sci U S A. 2000;97:4991–6. [PubMed: 10781110]

[62]. Cailliatte R, Schikora A, Briat JF, Mari S, Curie C. High-affinity manganese uptake by the metal transporter NRAMP1 is essential for Arabidopsis growth in low manganese conditions. Plant Cell. 2010;22:904–17. [PubMed: 20228245]

[63]. Curie C, Alonso JM, Le Jean M, Ecker JR, Briat JF. Involvement of NRAMP1 from *Arabidopsis thaliana* in iron transport. Biochem J. 2000;347 Pt 3:749–55. [PubMed: 10769179]

[64]. Peris-Peris C, Serra-Cardona A, Sanchez-Sanuy F, Campo S, Arino J, San Segundo B. Two NRAMP6 Isoforms Function as Iron and Manganese Transporters and Contribute to Disease Resistance in Rice. Mol Plant Microbe Interact. 2017;30:385–98. [PubMed: 28430017]

[65]. Sasaki A, Yamaji N, Yokosho K, Ma JF. Nramp5 is a major transporter responsible for manganese and cadmium uptake in rice. Plant Cell. 2012;24:2155–67. [PubMed: 22589467]

[66]. Segond D, Dellagi A, Lanquar V, Rigault M, Patrit O, Thomine S, et al. NRAMP genes function in *Arabidopsis thaliana* resistance to *Erwinia chrysanthemi* infection. Plant J. 2009;58:195–207. [PubMed: 19121106]

[67]. Ullah I, Wang Y, Eide DJ, Dunwell JM. Evolution, and functional analysis of Natural Resistance-Associated Macrophage Proteins (NRAMPs) from Theobroma cacao and their role in cadmium accumulation. Scientific Reports. 8.

[68]. Yamaji N, Sasaki A, Xia JX, Yokosho K, Ma JF. A node-based switch for preferential distribution of manganese in rice. Nat Commun. 2013;4:2442. [PubMed: 24048172]

[69]. Alejandro S, Cailliatte R, Alcon C, Dirick L, Domergue F, Correia D, et al. Intracellular Distribution of Manganese by the Trans-Golgi Network Transporter NRAMP2 Is Critical for Photosynthesis and Cellular Redox Homeostasis. Plant Cell. 2017;29:3068–84. [PubMed: 29180598]

[70]. Li JY, Liu J, Dong D, Jia X, McCouch SR, Kochian LV. Natural variation underlies alterations in Nramp aluminum transporter (NRAT1) expression and function that play a key role in rice aluminum tolerance. Proc Natl Acad Sci U S A. 2014;111:6503–8. [PubMed: 24728832]

[71]. Xia J, Yamaji N, Kasai T, Ma JF. Plasma membrane-localized transporter for aluminum in rice. Proc Natl Acad Sci U S A. 2010;107:18381–5. [PubMed: 20937890]

[72]. Alonso JM, Hirayama T, Roman G, Nourizadeh S, Ecker JR. EIN2, a bifunctional transducer of ethylene and stress responses in Arabidopsis. Science. 1999;284:2148–52. [PubMed: 10381874]

[73]. Agranoff D, Collins L, Kehres D, Harrison T, Maguire M, Krishna S. The Nramp orthologue of *Cryptococcus neoformans* is a pH-dependent transporter of manganese, iron, cobalt and nickel. Biochem J. 2005;385:225–32. [PubMed: 15350193]

[74]. Chen XZ, Peng JB, Cohen A, Nelson H, Nelson N, Hediger MA. Yeast SMF1 mediates H^+-coupled iron uptake with concomitant uncoupled cation currents. J Biol Chem. 1999;274:35089–94. [PubMed: 10574989]

[75]. Cohen A, Nelson H, Nelson N. The family of SMF metal ion transporters in yeast cells. J Biol Chem. 2000;275:33388–94. [PubMed: 10930410]

[76]. Pinner E, Gruenheid S, Raymond M, Gros P. Functional complementation of the yeast divalent cation transporter family SMF by NRAMP2, a member of the mammalian natural resistance-associated macrophage protein family. J Biol Chem. 1997;272:28933–8. [PubMed: 9360964]

[77]. Portnoy ME, Liu XF, Culotta VC. Saccharomyces cerevisiae expresses three functionally distinct homologues of the nramp family of metal transporters. Mol Cell Biol. 2000;20:7893–902. [PubMed: 11027260]

[78]. Au C, Benedetto A, Anderson J, Labrousse A, Erikson K, Ewbank JJ, et al. SMF-1, SMF-2 and SMF-3 DMT1 orthologues regulate and are regulated differentially by manganese levels in *C. elegans*. PLoS One. 2009;4:e7792. [PubMed: 19924247]

[79]. Martinez-Barnetche J, Garcia Solache M, Neri Lecona A, Tello Lopez AT, del Carmen Rodriguez M, Gamba G, et al. Cloning and functional characterization of the *Anopheles albimanus* DMT1/NRAMP homolog: implications in iron metabolism in mosquitoes. Insect Biochem Mol Biol. 2007;37:532–9. [PubMed: 17517330]

[80]. Neves JV, Wilson JM, Kuhl H, Reinhardt R, Castro LF, Rodrigues PN. Natural history of SLC11 genes in vertebrates: tales from the fish world. BMC Evol Biol. 2011;11:106. [PubMed: 21501491]

[81]. Montalbetti N, Simonin A, Kovacs G, Hediger MA. Mammalian iron transporters: families SLC11 and SLC40. Mol Asp Med. 2013;34:270–87.

[82]. Andrews NC. Forging a field: the golden age of iron biology. Blood. 2008;112:219–30. [PubMed: 18606887]

[83]. Coffey R, Ganz T. Iron homeostasis: An anthropocentric perspective. J Biol Chem. 2017;292:12727–34. [PubMed: 28615456]

[84]. Knutson MD. Iron transport proteins: Gateways of cellular and systemic iron homeostasis. J Biol Chem. 2017;292:12735–43. [PubMed: 28615441]

[85]. Johnson EE, Wessling-Resnick M. Iron metabolism and the innate immune response to infection. Microbes Infect. 2012;14:207–16. [PubMed: 22033148]

[86]. Cellier M, Govoni G, Vidal S, Kwan T, Groulx N, Liu J, et al. Human natural resistance-associated macrophage protein: cDNA cloning, chromosomal mapping, genomic organization, and tissue-specific expression. J Exp Med. 1994;180:1741–52. [PubMed: 7964458]

[87]. Vidal SM, Malo D, Vogan K, Skamene E, Gros P. Natural resistance to infection with intracellular parasites: isolation of a candidate for Bcg. Cell. 1993;73:469–85. [PubMed: 8490962]

[88]. Forbes JR, Gros P. Iron, manganese, and cobalt transport by Nramp1 (Slc11a1) and Nramp2 (Slc11a2) expressed at the plasma membrane. Blood. 2003;102:1884–92. [PubMed: 12750164]

[89]. Govoni G, Canonne-Hergaux F, Pfeifer CG, Marcus SL, Mills SD, Hackam DJ, et al. Functional expression of Nramp1 in vitro in the murine macrophage line RAW264.7. Infect Immun. 1999;67:2225–32. [PubMed: 10225878]

[90]. Jabado N, Jankowski A, Dougaparsad S, Picard V, Grinstein S, Gros P. Natural resistance to intracellular infections: natural resistance-associated macrophage protein 1 (Nramp1) functions as a pH-dependent manganese transporter at the phagosomal membrane. J Exp Med. 2000;192:1237–48. [PubMed: 11067873]

[91]. Cunrath O, Bumann D. Host resistance factor SLC11A1 restricts *Salmonella* growth through magnesium deprivation. Science. 2019;366:995–9. [PubMed: 31753999]

[92]. Lisher JP, Giedroc DP. Manganese acquisition and homeostasis at the host-pathogen interface. Front Cell Infect Microbiol. 2013;3:91. [PubMed: 24367765]

[93]. Hood MI, Skaar EP. Nutritional immunity: transition metals at the pathogen-host interface. Nat Rev Microbiol. 2012;10:525–37. [PubMed: 22796883]

[94]. Goswami T, Bhattacharjee A, Babal P, Searle S, Moore E, Li M, et al. Natural-resistance-associated macrophage protein 1 is an H^+/bivalent cation antiporter. Biochem J. 2001;354:511–9. [PubMed: 11237855]

[95]. Techau ME, Valdez-Taubas J, Popoff JF, Francis R, Seaman M, Blackwell JM. Evolution of differences in transport function in Slc11a family members. J Biol Chem. 2007;282:35646–56. [PubMed: 17932044]

[96]. Skamene E, Gros P, Forget A, Kongshavn PA, St Charles C, Taylor BA. Genetic regulation of resistance to intracellular pathogens. Nature. 1982;297:506–9. [PubMed: 7045675]

[97]. Vidal SM, Pinner E, Lepage P, Gauthier S, Gros P. Natural resistance to intracellular infections: Nramp1 encodes a membrane phosphoglycoprotein absent in macrophages from susceptible (Nramp1 D169) mouse strains. J Immunol. 1996;157:3559–68. [PubMed: 8871656]

[98]. Canonne-Hergaux F, Fleming MD, Levy JE, Gauthier S, Ralph T, Picard V, et al. The Nramp2/DMT1 iron transporter is induced in the duodenum of microcytic anemia mk mice but is not properly targeted to the intestinal brush border. Blood. 2000;96:3964–70. [PubMed: 11090085]

[99]. Canonne-Hergaux F, Gruenheid S, Ponka P, Gros P. Cellular and subcellular localization of the Nramp2 iron transporter in the intestinal brush border and regulation by dietary iron. Blood. 1999;93:4406–17. [PubMed: 10361139]

[100]. Knopfel M, Zhao L, Garrick MD. Transport of divalent transition-metal ions is lost in small-intestinal tissue of b/b Belgrade rats. Biochemistry. 2005;44:3454–65. [PubMed: 15736955]

[101]. Gunshin H, Allerson CR, Polycarpou-Schwarz M, Rofts A, Rogers JT, Kishi F, et al. Iron-dependent regulation of the divalent metal ion transporter. FEBS Lett. 2001;509:309–16. [PubMed: 11741608]

[102]. Hentze MW, Muckenthaler MU, Andrews NC. Balancing acts: molecular control of mammalian iron metabolism. Cell. 2004;117:285–97. [PubMed: 15109490]

[103]. Donovan A, Brownlie A, Zhou Y, Shepard J, Pratt SJ, Moynihan J, et al. Positional cloning of zebrafish ferroportin1 identifies a conserved vertebrate iron exporter. Nature. 2000;403:776–81. [PubMed: 10693807]

[104]. McKie AT, Marciani P, Rolfs A, Brennan K, Wehr K, Barrow D, et al. A novel duodenal iron-regulated transporter, IREG1, implicated in the basolateral transfer of iron to the circulation. Mol Cell. 2000;5:299–309. [PubMed: 10882071]

[105]. Vulpe CD, Kuo YM, Murphy TL, Cowley L, Askwith C, Libina N, et al. Hephaestin, a ceruloplasmin homologue implicated in intestinal iron transport, is defective in the sla mouse. Nature Genetics. 1999;21:195–9. [PubMed: 9988272]

[106]. Gkouvatsos K, Papanikolaou G, Pantopoulos K. Regulation of iron transport and the role of transferrin. Biochim Biophys Acta. 2012;1820:188–202. [PubMed: 22085723]

[107]. Ohgami RS, Campagna DR, Greer EL, Antiochos B, McDonald A, Chen J, et al. Identification of a ferrireductase required for efficient transferrin-dependent iron uptake in erythroid cells. Nat Genet. 2005;37:1264–9. [PubMed: 16227996]

[108]. Ohgami RS, Campagna DR, McDonald A, Fleming MD. The Steap proteins are metalloreductases. Blood. 2006;108:1388–94. [PubMed: 16609065]

[109]. Mackenzie B, Takanaga H, Hubert N, Rolfs A, Hediger MA. Functional properties of multiple isoforms of human divalent metal-ion transporter 1 (DMT1). Biochem J. 2007;403:59–69. [PubMed: 17109629]

[110]. Touret N, Furuya W, Forbes J, Gros P, Grinstein S. Dynamic traffic through the recycling compartment couples the metal transporter Nramp2 (DMT1) with the transferrin receptor. J Biol Chem. 2003;278:25548–57. [PubMed: 12724326]

[111]. Gruenheid S, Canonne-Hergaux F, Gauthier S, Hackam DJ, Grinstein S, Gros P. The iron transport protein NRAMP2 is an integral membrane glycoprotein that colocalizes with transferrin in recycling endosomes. J Exp Med. 1999;189:831–41. [PubMed: 10049947]

[112]. Hubert N, Hentze MW. Previously uncharacterized isoforms of divalent metal transporter (DMT)-1: implications for regulation and cellular function. Proc Natl Acad Sci U S A. 2002;99:12345–50. [PubMed: 12209011]

[113]. Tabuchi M, Tanaka N, Nishida-Kitayama J, Ohno H, Kishi F. Alternative splicing regulates the subcellular localization of divalent metal transporter 1 isoforms. Mol Biol Cell. 2002;13:4371–87. [PubMed: 12475959]

[114]. Shaw GC, Cope JJ, Li L, Corson K, Hersey C, Ackermann GE, et al. Mitoferrin is essential for erythroid iron assimilation. Nature. 2006;440:96–100. [PubMed: 16511496]

[115]. Wolff NA, Garrick LM, Zhao L, Garrick MD, Thevenod F. Mitochondria represent another locale for the divalent metal transporter 1 (DMT1). Channels. 2014;8:458–66. [PubMed: 25483589]

[116]. Wolff NA, Garrick MD, Zhao L, Garrick LM, Ghio AJ, Thevenod F. A role for divalent metal transporter (DMT1) in mitochondrial uptake of iron and manganese. Sci Rep. 2018;8:211. [PubMed: 29317744]

[117]. Jabado N, Canonne-Hergaux F, Gruenheid S, Picard V, Gros P. Iron transporter Nramp2/DMT-1 is associated with the membrane of phagosomes in macrophages and Sertoli cells. Blood. 2002;100:2617–22. [PubMed: 12239176]

[118]. Soe-Lin S, Apte SS, Andriopoulos B Jr., Andrews MC, Schranzhofer M, Kahawita T, et al. Nramp1 promotes efficient macrophage recycling of iron following erythrophagocytosis in vivo. Proc Natl Acad Sci U S A. 2009;106:5960–5. [PubMed: 19321419]

[119]. Soe-Lin S, Apte SS, Mikhael MR, Kayembe LK, Nie G, Ponka P. Both Nramp1 and DMT1 are necessary for efficient macrophage iron recycling. Exp Hematol. 2010;38:609–17. [PubMed: 20394798]

[120]. Delaby C, Rondeau C, Pouzet C, Willemetz A, Pilard N, Desjardins M, et al. Subcellular localization of iron and heme metabolism related proteins at early stages of erythrophagocytosis. PLoS One. 2012;7:e42199. [PubMed: 22860081]

[121]. Fleming MD, Romano MA, Su MA, Garrick LM, Garrick MD, Andrews NC. Nramp2 is mutated in the anemic Belgrade (b) rat: evidence of a role for Nramp2 in endosomal iron transport. Proc Natl Acad Sci U S A. 1998;95:1148–53. [PubMed: 9448300]

[122]. Fleming MD, Trenor CC, Su MA, Foernzler D, Beier DR, Dietrich WF, et al. Microcytic anaemia mice have a mutation in Nramp2, a candidate iron transporter gene. Nature Genetics. 1997;16:383–6. [PubMed: 9241278]

[123]. Canonne-Hergaux F, Zhang AS, Ponka P, Gros P. Characterization of the iron transporter DMT1 (NRAMP2/DCT1) in red blood cells of normal and anemic mk/mk mice. Blood. 2001;98:3823–30. [PubMed: 11739192]

[124]. Su MA, Trenor CC, Fleming JC, Fleming MD, Andrews NC. The G185R mutation disrupts functions of the iron transporter Nramp2. Blood. 1998;92:2157–63. [PubMed: 9731075]

[125]. Blanco E, Kannengiesser C, Grandchamp B, Tasso M, Beaumont C. Not all DMT1 mutations lead to iron overload. Blood Cells Mol Dis. 2009;43:199–201. [PubMed: 19553145]

[126]. Mims MP, Guan Y, Pospisilova D, Priwitzerova M, Indrak K, Ponka P, et al. Identification of a human mutation of DMT1 in a patient with microcytic anemia and iron overload. Blood. 2005;105:1337–42. [PubMed: 15459009]

[127]. Gunshin H, Fujiwara Y, Custodio AO, Direnzo C, Robine S, Andrews NC. Slc11a2 is required for intestinal iron absorption and erythropoiesis but dispensable in placenta and liver. J Clin Invest. 2005;115:1258–66. [PubMed: 15849611]

[128]. Shawki A, Anthony SR, Nose Y, Engevik MA, Niespodzany EJ, Barrientos T, et al. Intestinal DMT1 is critical for iron absorption in the mouse but is not required for the absorption of copper or manganese. American journal of physiology Gastrointestinal and liver physiology. 2015;309:G635–47. [PubMed: 26294671]

[129]. Courville P, Chaloupka R, Cellier MF. Recent progress in structure-function analyses of Nramp proton-dependent metal-ion transporters. Biochem Cell Biol. 2006;84:960–78. [PubMed: 17215883]

[130]. Nevo Y, Nelson N. The NRAMP family of metal-ion transporters. Biochim Biophys Acta. 2006;1763:609–20. [PubMed: 16908340]

[131]. Shawki A, Knight PB, Maliken BD, Niespodzany EJ, Mackenzie B. H^+-coupled divalent metal-ion transporter-1: functional properties, physiological roles and therapeutics. Curr Top Membr. 2012;70:169–214. [PubMed: 23177986]

[132]. Bozzi AT, Bane LB, Zimanyi CM, Gaudet R. Unique structural features in an Nramp metal transporter impart substrate-specific proton co-transport and a kinetic bias to favor import. J Gen Physiol. 2019;151:1413–29. [PubMed: 31619456]

[133]. Bozzi AT, Bane LB, Weihofen WA, McCabe AL, Singharoy A, Chipot CJ, et al. Conserved methionine dictates substrate preference in Nramp-family divalent metal transporters. Proc Natl Acad Sci U S A. 2016;113:10310–5. [PubMed: 27573840]

[134]. Bozzi AT, Bane LB, Weihofen WA, Singharoy A, Guillen ER, Ploegh HL, et al. Crystal Structure and Conformational Change Mechanism of a Bacterial Nramp-Family Divalent Metal Transporter. Structure. 2016;24:2102–14. [PubMed: 27839948]

[135]. Bozzi AT, McCabe AL, Barnett BC, Gaudet R. Transmembrane helix 6b links proton and metal release pathways and drives conformational change in an Nramp-family transition metal transporter. J Biol Chem. 2020;295:1212–24. [PubMed: 31882536]

[136]. Bozzi AT, Zimanyi CM, Nicoludis JM, Lee BK, Zhang CH, Gaudet R. Structures in multiple conformations reveal distinct transition metal and proton pathways in an Nramp transporter. eLife. 2019;8:e41124. [PubMed: 30714568]

[137]. Courville P, Chaloupka R, Veyrier F, Cellier MF. Determination of transmembrane topology of the *Escherichia coli* natural resistance-associated macrophage protein (Nramp) ortholog. J Biol Chem. 2004;279:3318–26. [PubMed: 14607838]

[138]. Czachorowski M, Lam-Yuk-Tseung S, Cellier M, Gros P. Transmembrane topology of the mammalian Slc11a2 iron transporter. Biochemistry. 2009;48:8422–34. [PubMed: 19621945]

[139]. Ehrnstorfer IA, Geertsma ER, Pardon E, Steyaert J, Dutzler R. Crystal structure of a SLC11 (NRAMP) transporter reveals the basis for transition-metal ion transport. Nat Struct Mol Biol. 2014;21:990–6. [PubMed: 25326704]

[140]. Ehrnstorfer IA, Manatschal C, Arnold FM, Laederach J, Dutzler R. Structural and mechanistic basis of proton-coupled metal ion transport in the SLC11/NRAMP family. Nat Commun. 2017;8:14033. [PubMed: 28059071]

[141]. Manatschal C, Pujol-Gimenez J, Poirier M, Reymond JL, Hediger MA, Dutzler R. Mechanistic basis of the inhibition of SLC11/NRAMP-mediated metal ion transport by bis-isothiourea substituted compounds. eLife. 2019;8.

[142]. Courville P, Urbankova E, Rensing C, Chaloupka R, Quick M, Cellier MF. Solute carrier 11 cation symport requires distinct residues in transmembrane helices 1 and 6. J Biol Chem. 2008;283:9651–8. [PubMed: 18227061]

[143]. Cellier MF. Nutritional immunity: homology modeling of Nramp metal import. Advances in experimental medicine and biology. 2012;946:335–51. [PubMed: 21948377]

[144]. Xu H, Jin J, DeFelice LJ, Andrews NC, Clapham DE. A spontaneous, recurrent mutation in divalent metal transporter-1 exposes a calcium entry pathway. PLoS Biol. 2004;2:E50. [PubMed: 15024413]

[145]. Haemig HA, Moen PJ, Brooker RJ. Evidence that highly conserved residues of transmembrane segment 6 of *Escherichia coli* MntH are important for transport activity. Biochemistry. 2010;49:4662–71. [PubMed: 20441230]

[146]. Krishnamurthy H, Gouaux E. X-ray structures of LeuT in substrate-free outward-open and apo inward-open states. Nature. 2012;481:469–74. [PubMed: 22230955]

[147]. Kazmier K, Sharma S, Islam SM, Roux B, McHaourab HS. Conformational cycle and ion-coupling mechanism of the Na^+/hydantoin transporter Mhp1. Proc Natl Acad Sci U S A. 2014;111:14752–7. [PubMed: 25267652]

[148]. Shimamura T, Weyand S, Beckstein O, Rutherford NG, Hadden JM, Sharples D, et al. Molecular basis of alternating access membrane transport by the sodium-hydantoin transporter Mhp1. Science. 2010;328:470–3. [PubMed: 20413494]

[149]. Perez C, Koshy C, Yildiz O, Ziegler C. Alternating-access mechanism in conformationally asymmetric trimers of the betaine transporter BetP. Nature. 2012;490:126–30. [PubMed: 22940865]

[150]. Coleman JA, Gouaux E. Structural basis for recognition of diverse antidepressants by the human serotonin transporter. Nat Struct Mol Biol. 2018;25:170–5. [PubMed: 29379174]

[151]. Coleman JA, Green EM, Gouaux E. X-ray structures and mechanism of the human serotonin transporter. Nature. 2016;532:334–9. [PubMed: 27049939]

[152]. Kazmier K, Sharma S, Quick M, Islam SM, Roux B, Weinstein H, et al. Conformational dynamics of ligand-dependent alternating access in LeuT. Nat Struct Mol Biol. 2014;21:472–9. [PubMed: 24747939]

[153]. Forrest LR, Rudnick G. The rocking bundle: a mechanism for ion-coupled solute flux by symmetrical transporters. Physiology (Bethesda). 2009;24:377–86. [PubMed: 19996368]

[154]. Cohen A, Nevo Y, Nelson N. The first external loop of the metal ion transporter DCT1 is involved in metal ion binding and specificity. Proc Natl Acad Sci U S A. 2003;100:10694–9. [PubMed: 12954986]

[155]. Nevo Y. Site-directed mutagenesis investigation of coupling properties of metal ion transport by DCT1. Biochim Biophys Acta. 2008;1778:334–41. [PubMed: 17980698]

[156]. Picard V, Govoni G, Jabado N, Gros P. Nramp 2 (DCT1/DMT1) expressed at the plasma membrane transports iron and other divalent cations into a calcein-accessible cytoplasmic pool. J Biol Chem. 2000;275:35738–45. [PubMed: 10942769]

[157]. Pujol-Gimenez J, Hediger MA, Gyimesi G. A novel proton transfer mechanism in the SLC11 family of divalent metal ion transporters. Sci Rep. 2017;7:6194. [PubMed: 28754960]

[158]. Tandy S, Williams M, Leggett A, Lopez-Jimenez M, Dedes M, Ramesh B, et al. Nramp2 expression is associated with pH-dependent iron uptake across the apical membrane of human intestinal Caco-2 cells. J Biol Chem. 2000;275:1023–9. [PubMed: 10625641]

[159]. Okubo M, Yamada K, Hosoyamada M, Shibasaki T, Endou H. Cadmium transport by human Nramp 2 expressed in Xenopus laevis oocytes. Toxicology and applied pharmacology. 2003;187:162–7. [PubMed: 12662899]

[160]. Worthington MT, Browne L, Battle EH, Luo RQ. Functional properties of transfected human DMT1 iron transporter. American journal of physiology Gastrointestinal and liver physiology. 2000;279:G1265–73. [PubMed: 11093950]

[161]. Illing AC, Shawki A, Cunningham CL, Mackenzie B. Substrate profile and metal-ion selectivity of human divalent metal-ion transporter-1. J Biol Chem. 2012;287:30485–96. [PubMed: 22736759]

[162]. Marciani P, Trotti D, Hediger MA, Monticelli G. Modulation of DMT1 activity by redox compounds. J Membr Biol. 2004;197:91–9. [PubMed: 15014911]

[163]. Nevo Y, Nelson N. The mutation F227I increases the coupling of metal ion transport in DCT1. J Biol Chem. 2004;279:53056–61. [PubMed: 15475345]

[164]. Bannon DI, Abounader R, Lees PS, Bressler JP. Effect of DMT1 knockdown on iron, cadmium, and lead uptake in Caco-2 cells. Am J Physiol Cell Physiol. 2003;284:C44–50. [PubMed: 12388109]

[165]. Bannon DI, Portnoy ME, Olivi L, Lees PSJ, Culotta VC, Bressler JP. Uptake of lead and iron by divalent metal transporter 1 in yeast and mammalian cells. Biochemical and Biophysical Research Communications. 2002;295:978–84. [PubMed: 12127992]

[166]. Vazquez M, Velez D, Devesa V, Puig S. Participation of divalent cation transporter DMT1 in the uptake of inorganic mercury. Toxicology. 2015;331:119–24. [PubMed: 25772431]

[167]. Arredondo M, Mendiburo MJ, Flores S, Singleton ST, Garrick MD. Mouse divalent metal transporter 1 is a copper transporter in HEK293 cells. Biometals. 2014;27:115–23. [PubMed: 24327293]

[168]. Shawki A, Mackenzie B. Interaction of calcium with the human divalent metal-ion transporter-1. Biochem Biophys Res Commun. 2010;393:471–5. [PubMed: 20152801]

[169]. Sacher A, Cohen A, Nelson N. Properties of the mammalian and yeast metal-ion transporters DCT1 and Smf1p expressed in *Xenopus laevis* oocytes. J Exp Biol. 2001;204:1053–61. [PubMed: 11222124]

[170]. Buracco S, Peracino B, Cinquetti R, Signoretto E, Vollero A, Imperiali F, et al. *Dictyostelium* Nramp1, which is structurally and functionally similar to mammalian DMT1 transporter, mediates phagosomal iron efflux. J Cell Sci. 2015;128:3304–16. [PubMed: 26208637]

[171]. Pottier M, Oomen R, Picco C, Giraudat J, Scholz-Starke J, Richaud P, et al. Identification of mutations allowing Natural Resistance Associated Macrophage Proteins (NRAMP) to discriminate against cadmium. Plant J. 2015;83:625–37. [PubMed: 26088788]

[172]. Li J, Wang L, Zheng L, Wang Y, Chen X, Zhang W. A Functional Study Identifying Critical Residues Involving Metal Transport Activity and Selectivity in Natural Resistance-Associated Macrophage Protein 3 in *Arabidopsis thaliana*. Int J Mol Sci. 2018;19.

[173]. Mizuno T, Usui K, Horie K, Nosaka S, Mizuno N, Obata H. Cloning of three ZIP/Nramp transporter genes from a Ni hyperaccumulator plant *Thlaspi japonicum* and their Ni^{2+}-transport abilities. Plant physiology and biochemistry : PPB. 2005;43:793–801. [PubMed: 16198592]

[174]. Tiwari M, Sharma D, Dwivedi S, Singh M, Tripathi RD, Trivedi PK. Expression in Arabidopsis and cellular localization reveal involvement of rice NRAMP, OsNRAMP1, in arsenic transport and tolerance. Plant Cell Environ. 2014;37:140–52. [PubMed: 23700971]

[175]. Yokosho K, Yamaji N, Ma JF. Buckwheat FeNramp5 mediates high Mn uptake in roots. Plant Cell Physiol. 2020.

[176]. Ueki T, Furuno N, Michibata H. A novel vanadium transporter of the Nramp family expressed at the vacuole of vanadium-accumulating cells of the ascidian *Ascidia sydneiensis samea*. Biochim Biophys Acta. 2011;1810:457–64. [PubMed: 21236319]

[177]. Chaloupka R, Courville P, Veyrier F, Knudsen B, Tompkins TA, Cellier MF. Identification of functional amino acids in the Nramp family by a combination of evolutionary analysis and biophysical studies of metal and proton cotransport in vivo. Biochemistry. 2005;44:726–33. [PubMed: 15641799]

[178]. Haemig HA, Brooker RJ. Importance of conserved acidic residues in mntH, the Nramp homolog of *Escherichia coli*. J Membr Biol. 2004;201:97–107. [PubMed: 15630547]

[179]. Gantner M, Laftsoglou T, Rong H, Postis VLG, Jeuken LJC. Electrophysiology Measurements of Metal Transport by MntH2 from Enterococcus faecalis. Membranes (Basel). 2020;10.

[180]. Mackenzie B, Ujwal ML, Chang MH, Romero MF, Hediger MA. Divalent metal-ion transporter DMT1 mediates both H^+-coupled Fe^{2+} transport and uncoupled fluxes. Pflugers Arch. 2006;451:544–58. [PubMed: 16091957]

[181]. Lan W, Ren H, Pang Y, Huang C, Xu Y, Brooker RJ, et al. A facile transport assay for H^+ coupled membrane transport using fluorescence probes. Anal Methods. 2012;4:44–6.

[182]. Chandrangsu P, Rensing C, Helmann JD. Metal homeostasis and resistance in bacteria. Nat Rev Microbiol. 2017;15:338–50. [PubMed: 28344348]

[183]. Lam-Yuk-Tseung S, Govoni G, Forbes J, Gros P. Iron transport by Nramp2/DMT1: pH regulation of transport by 2 histidines in transmembrane domain 6. Blood. 2003;101:3699–707. [PubMed: 12522007]

[184]. Lin Z, Fernandez-Robledo JA, Cellier MF, Vasta GR. The natural resistance-associated macrophage protein from the protozoan parasite *Perkinsus marinus* mediates iron uptake. Biochemistry. 2011;50:6340–55. [PubMed: 21661746]

[185]. Shin JH, Wakeman CA, Goodson JR, Rodionov DA, Freedman BG, Senger RS, et al. Transport of magnesium by a bacterial Nramp-related gene. PLoS Genet. 2014;10:e1004429. [PubMed: 24968120]

[186]. Lu M, Yang G, Li P, Wang Z, Fu S, Zhang X, et al. Bioinformatic and Functional Analysis of a Key Determinant Underlying the Substrate Selectivity of the Al Transporter, Nrat1. Front Plant Sci. 2018;9:606. [PubMed: 29868064]

[187]. Mangold S, Potrykus J, Bjorn E, Lovgren L, Dopson M. Extreme zinc tolerance in acidophilic microorganisms from the bacterial and archaeal domains. Extremophiles. 2013;17:75–85. [PubMed: 23143658]

[188]. Sun GL, Reynolds EE, Belcher AM. Designing yeast as plant-like hyperaccumulators for heavy metals. Nat Commun. 2019;10:5080. [PubMed: 31704944]

[189]. Bot CT, Prodan C. Quantifying the membrane potential during *E. coli* growth stages. Biophys Chem. 2010;146:133–7. [PubMed: 20031298]

[190]. Zhang AS, Canonne-Hergaux F, Gruenheid S, Gros P, Ponka P. Use of Nramp2-transfected Chinese hamster ovary cells and reticulocytes from mk/mk mice to study iron transport mechanisms. Exp Hematol. 2008;36:1227–35. [PubMed: 18722041]

[191]. Elisma F, Jumarie C. Evidence for cadmium uptake through Nramp2: metal speciation studies with Caco-2 cells. Biochem Biophys Res Commun. 2001;285:662–8. [PubMed: 11453644]

[192]. Nelson N, Sacher A, Nelson H. The significance of molecular slips in transport systems. Nat Rev Mol Cell Biol. 2002;3:876–81. [PubMed: 12415305]

[193]. Daly MJ, Gaidamakova EK, Matrosova VY, Vasilenko A, Zhai M, Venkateswaran A, et al. Accumulation of Mn(II) in *Deinococcus radiodurans* facilitates gamma-radiation resistance. Science. 2004;306:1025–8. [PubMed: 15459345]

[194]. Cellier MFM. Evolutionary analysis of Slc11 mechanism of proton-coupled metal-ion transmembrane import. AIMS Biophysics. 2016;3:286–318.

[195]. Malinauskaite L, Said S, Sahin C, Grouleff J, Shahsavar A, Bjerregaard H, et al. A conserved leucine occupies the empty substrate site of LeuT in the Na^+-free return state. Nat Commun. 2016;7:11673. [PubMed: 27221344]

[196]. Shaffer PL, Goehring A, Shankaranarayanan A, Gouaux E. Structure and mechanism of a Na^+-independent amino acid transporter. Science. 2009;325:1010–4. [PubMed: 19608859]

[197]. Shi L, Weinstein H. Conformational rearrangements to the intracellular open states of the LeuT and ApcT transporters are modulated by common mechanisms. Biophys J. 2010;99:L103–5. [PubMed: 21156121]

[198]. Zhao Y, Quick M, Shi L, Mehler EL, Weinstein H, Javitch JA. Substrate-dependent proton antiport in neurotransmitter:sodium symporters. Nat Chem Biol. 2010;6:109–16. [PubMed: 20081826]

[199]. Isom DG, Castaneda CA, Cannon BR, Velu PD, Garcia-Moreno EB. Charges in the hydrophobic interior of proteins. Proc Natl Acad Sci U S A. 2010;107:16096–100. [PubMed: 20798341]

[200]. Rudnick G. Unconventional transport of metal ions and protons by Nramps. J Gen Physiol. 2019;151:1339–42. [PubMed: 31690583]

[201]. Hekstra DR, White KI, Socolich MA, Henning RW, Srajer V, Ranganathan R. Electric-field-stimulated protein mechanics. Nature. 2016;540:400–5. [PubMed: 27926732]

[202]. Llorente-Esteban A, Manville RW, Reyna-Neyra A, Abbott GW, Amzel LM, Carrasco N. Allosteric regulation of mammalian Na^+/I^- symporter activity by perchlorate. Nat Struct Mol Biol. 2020;27:533–9. [PubMed: 32451489]

[203]. Chen XZ, Zhu T, Smith DE, Hediger MA. Stoichiometry and kinetics of the high-affinity H+-coupled peptide transporter PepT2. J Biol Chem. 1999;274:2773–9. [PubMed: 9915809]

[204]. Mackenzie B, Shawki A, Ghio AJ, Stonehuerner JD, Zhao L, Ghadersohi S, et al. Calcium-channel blockers do not affect iron transport mediated by divalent metal-ion transporter-1. Blood. 2010;115:4148–9. [PubMed: 20489062]

[205]. Lam-Yuk-Tseung S, Mathieu M, Gros P. Functional characterization of the E399D DMT1/NRAMP2/SLC11A2 protein produced by an exon 12 mutation in a patient with microcytic anemia and iron overload. Blood Cells Mol Dis. 2005;35:212–6. [PubMed: 16023393]

[206]. Priwitzerova M, Nie G, Sheftel AD, Pospisilova D, Divoky V, Ponka P. Functional consequences of the human DMT1 (SLC11A2) mutation on protein expression and iron uptake. Blood. 2005;106:3985–7. [PubMed: 16091455]

[207]. Di Tommaso P, Moretti S, Xenarios I, Orobitg M, Montanyola A, Chang JM, et al. T-Coffee: a web server for the multiple sequence alignment of protein and RNA sequences using structural information and homology extension. Nucleic Acids Res. 2011;39:W13–7. [PubMed: 21558174]

[208]. Robert X, Gouet P. Deciphering key features in protein structures with the new ENDscript server. Nucleic Acids Res. 2014;42:W320–4. [PubMed: 24753421]

Highlights

- Nramp transporters import transition metal ions in many physiological contexts
- Nramps adopt a LeuT fold with adaptations including an intramembrane polar network
- The polar network enables H^+ cotransport and determines pH and voltage dependence
- Alternating access in Nramps depends largely on motions of TMs 1, 5, 6, and 10
- Nramps use a methionine to discriminate against alkaline earth metal ions

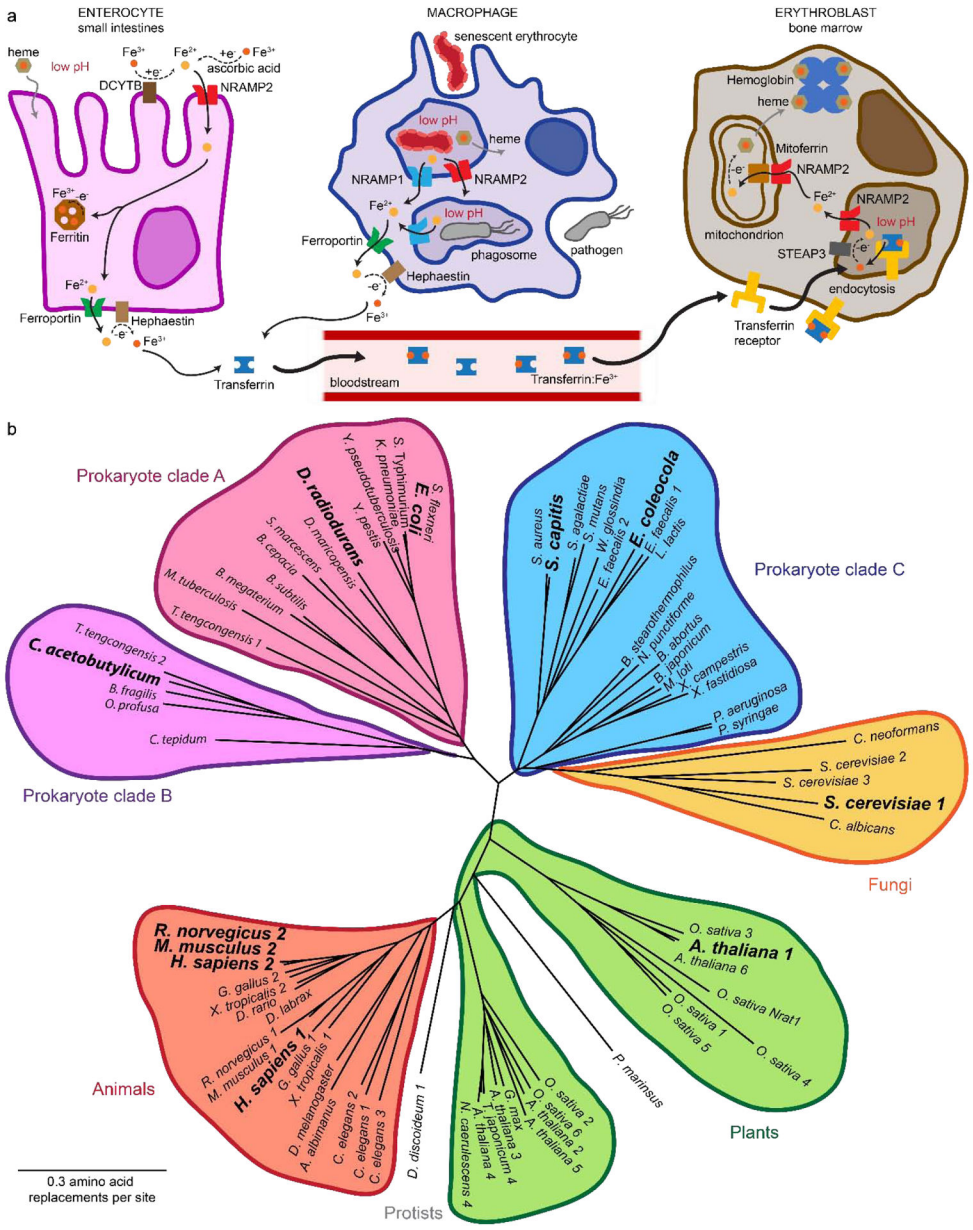

Figure 1. Functions and Evolution of the Nramp family.

(a) Known roles for Nramps in mammalian iron metabolism. In the acidic environment of the small intestines (Left), Fe^{3+} is reduced to Fe^{2+} by the duodenal cytochrome DCYTB or dietary ascorbic acid, then transported by NRAMP2 across the apical membrane to the enterocyte's cytosol, where it can be oxidized and stored in ferritin or exported to the bloodstream via ferroportin. In the acidified phagosomes of macrophages (Upper center), free Fe^{2+} released from dying red blood cells or engulfed pathogens is extracted by NRAMP1 (and perhaps NRAMP2) to the cytosol and subsequently exported through ferroportin. Exported Fe^{2+} is oxidized by hephaestin to Fe^{3+}, which then tightly binds to transferrin for distribution throughout the body (Lower center). At a destination cell such as a red blood cell precursor (Right), transferrin is endocytosed into an acidic endosome to

release Fe^{3+}, which is then reduced to Fe^{2+} by STEAP3 and transported by NRAMP2 to the cytosol. Fe^{2+} is then transported by NRAMP2 across the outer mitochondrial membrane and through mitoferrin into the mitochondrial matrix, where it can be oxidized and incorporated into heme. (b) A phylogenetic tree of a sampling of Nramp homologs illustrates the Nramp family's evolutionary divergence into several major clades for prokaryotes, fungi, plants, and animals. Sequences were aligned using Geneious version 9.1 (Biomatters) and the BLOSUM62 matrix. Model homologs discussed in the text and aligned in Figure 2 are in bold.

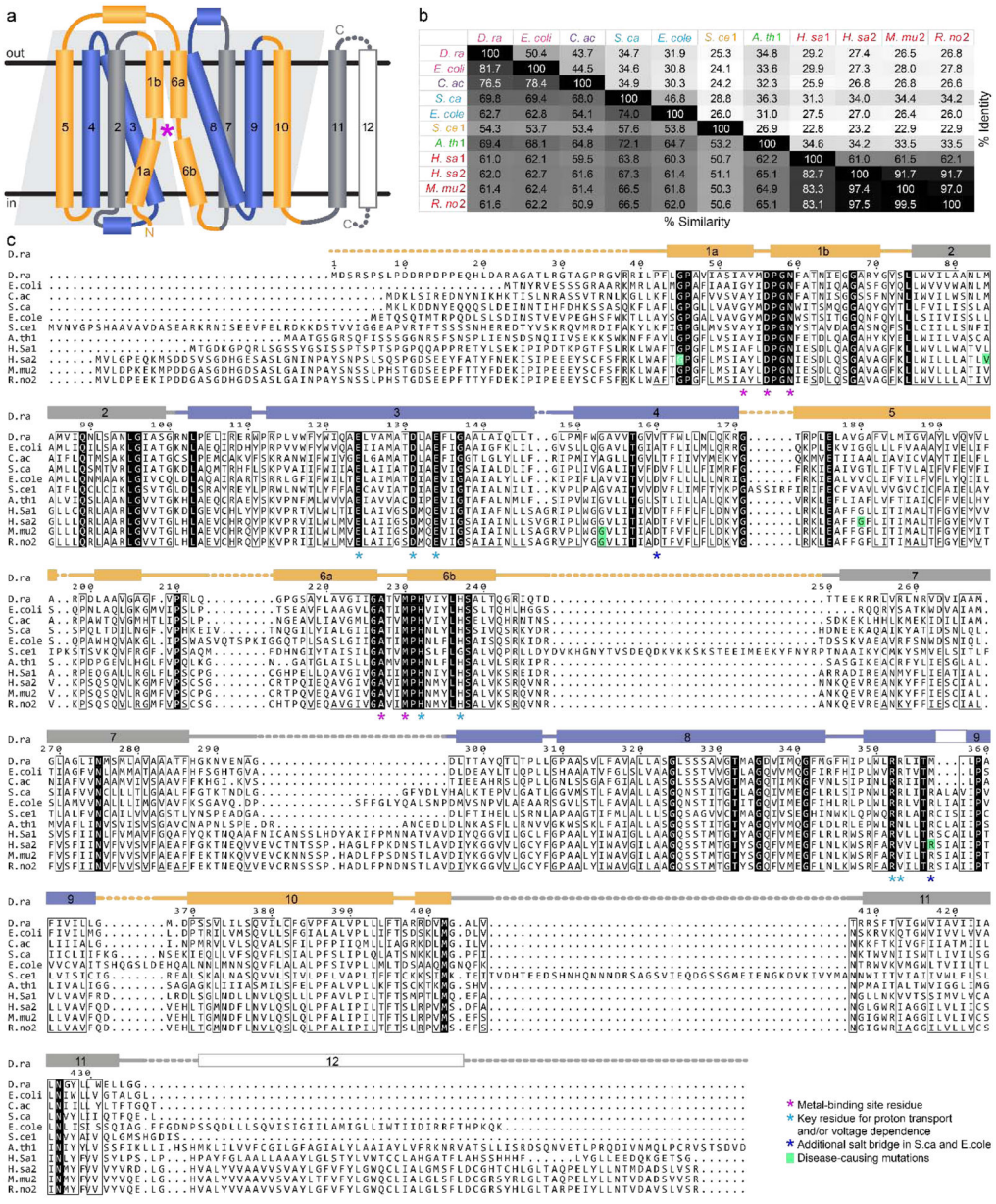

Figure 2. Sequence alignment of Nramp model systems and other clade-representative homologs.

(a) The Nramp secondary structure displays the characteristic topology of the LeuT fold, with TMs 1–5 and 6–10 comprising the two pseudosymmetric inverted repeats that intertwine in the tertiary structure. * denotes the location of the metal-binding site. TMs 1, 5, 6, and 10 are gold; TMs 3, 4, 8, and 9 are blue; TMs 2, 7, and 11 are gray. The same color scheme is used in later structure and model figures. Some homologs, including most eukaryotic Nramps and EcoleNramp [140], have a 12th TM helix. (b) Comparison of sequence conservation among Nramp model systems and other clade-representative homologs. The percent identity is plotted in the top right of the matrix, and similarity in the bottom left (calculated using the BLOSUM62 scale). (c) Aligned sequences of these model homologs. The numbering and secondary structure of DraNramp are included above the

alignment. Key residues for metal binding (magenta asterisks), proton transport and/or voltage dependence (cyan asterisks; blue asterisks indicate additional salt bridge in some homologs), and disease-causing mutation positions discussed in the main text (green highlight) are marked. Sequences were aligned using PSI/TM-Coffee [207] followed by manual editing of the N- and C-termini and some of the gap regions, and the alignment formatted with ESPript [208]. Uniprot accession numbers for the aligned sequences are: DraNramp (Q9RTP8), EcoliNramp (P0A769), *Clostridium acetobutylicum* MntH (Q97TN5; included as a representative of bacterial clade B), EcoleNramp (E4KPW4), ScaNramp (A0A0S4MEX1), *S. cerevisiae* Smf1p (C7GUZ9), Arabidopsis NRAMP1 (Q9SAH8), human NRAMP1 (P49279), mouse NRAMP2 (P49282), rat NRAMP2 (O54902), human NRAMP2 (P49281).

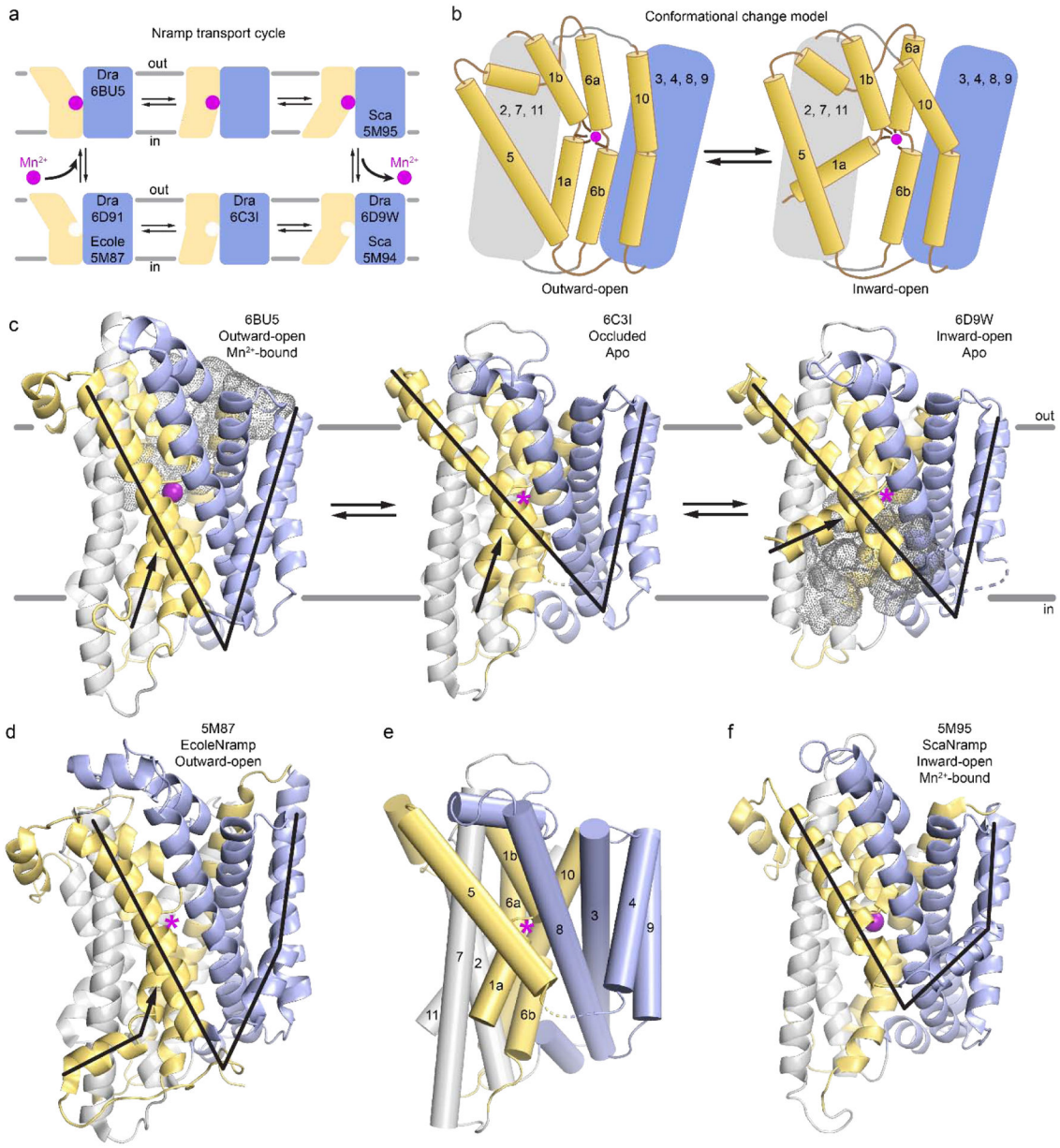

Figure 3. Nramp crystal structures capture multiple stages of the transport cycle.

(a) Cartoon depiction of metal ion transport cycle by Nramps, with gold and blue lobes representing the mobile and stationary parts of the protein, respectively. Cartoons are labeled with currently available crystal structures. (b) A schematic representation of the main conformational changes in DraNramp between the outward- and inward-open states, reorienting TMs 1, 5, 6, and 10 (yellow; as illustrated, all but TM6b reorient to some extent). Metal binding may trigger the toppling of TM10 as well as TM6a's inward movement to close off the outward metal-permeation pathway, with the latter motion propagated through extracellular loop 5–6 to pull on TM5 and thus begin to open the inner gate. TM1a must then displace significantly to fully expose the metal-binding site to the cytosol. (c) Crystal structures of DraNramp in three distinct states (PDB IDs: 6BU5, 6C3I, 6D91), with the

outward and inward vestibules shown in gray dot surface. The changes in orientation of TM1a and TM4-TM5 are highlighted with an arrow and black lines, respectively. (d) Structure of outward-open EcoleNramp (PDB ID: 5M87), highlighting it similarities to the analogous DraNramp structure above. (e) A cylinder representation of the occluded DraNramp (PDB ID: 6C3I) with helices labeled, for comparisons of the Nramp fold to panels (b), (d), and (f). (f) Structure of inward-open ScaNramp (PDB ID: 5M95), highlighting its similarities to the analogous DraNramp structure above. Note that TM1a was deleted in the crystallized construct. All structures in panels (c)–(f) were superimposed using only the blue-colored regions (TMs 3, 4, 8, 9). Manganese ions are shown as magenta spheres, and empty metal-binding sites denoted by magenta asterisks.

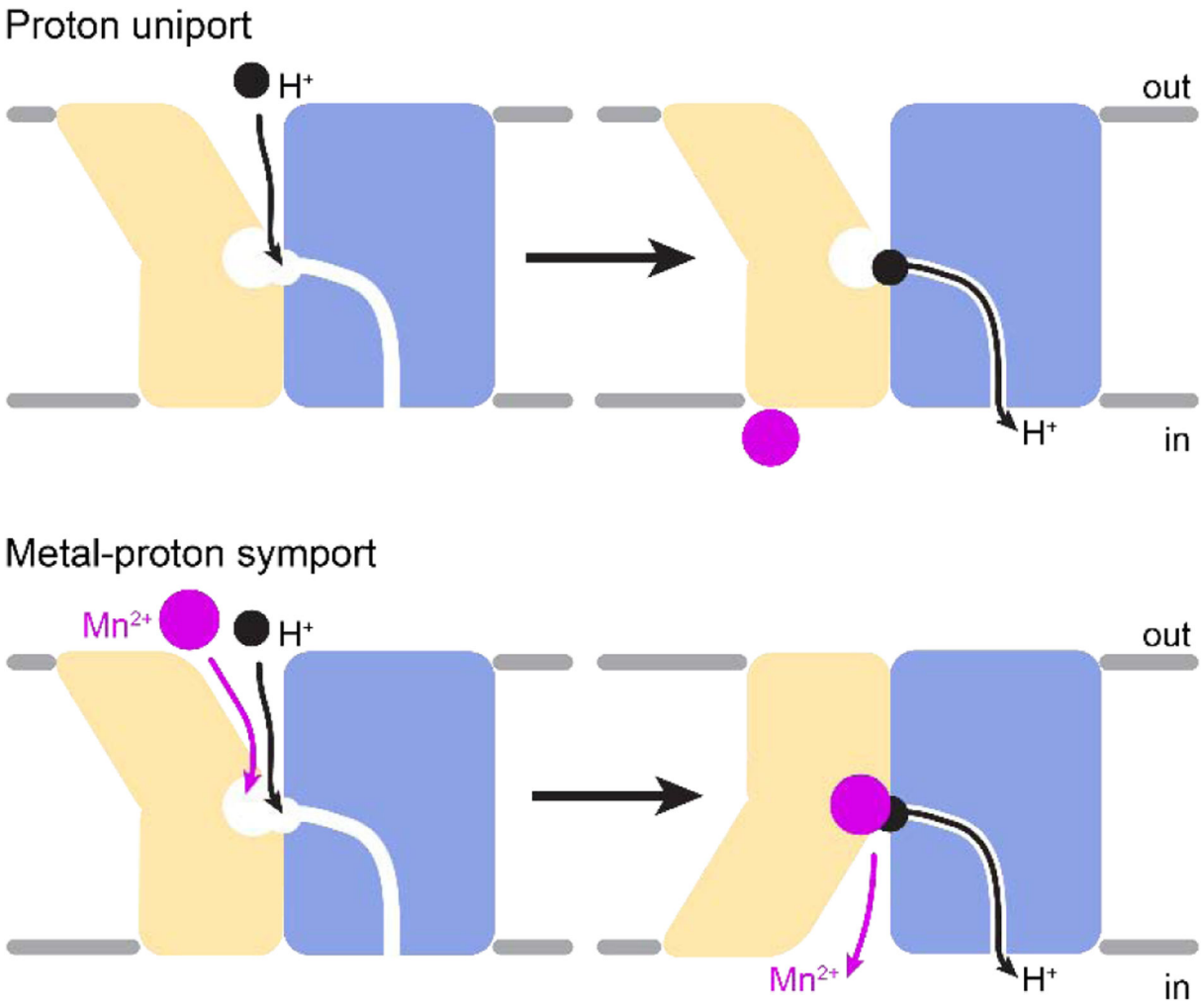

Figure 4. Modes of proton transport by DraNramp.

Proton transport occurs through the outward-open state, perhaps requiring subtle rearrangements. In contrast, metal transport requires bulk conformational change to the inward-open state. Figures adapted from Bozzi et al. 2019 [136].

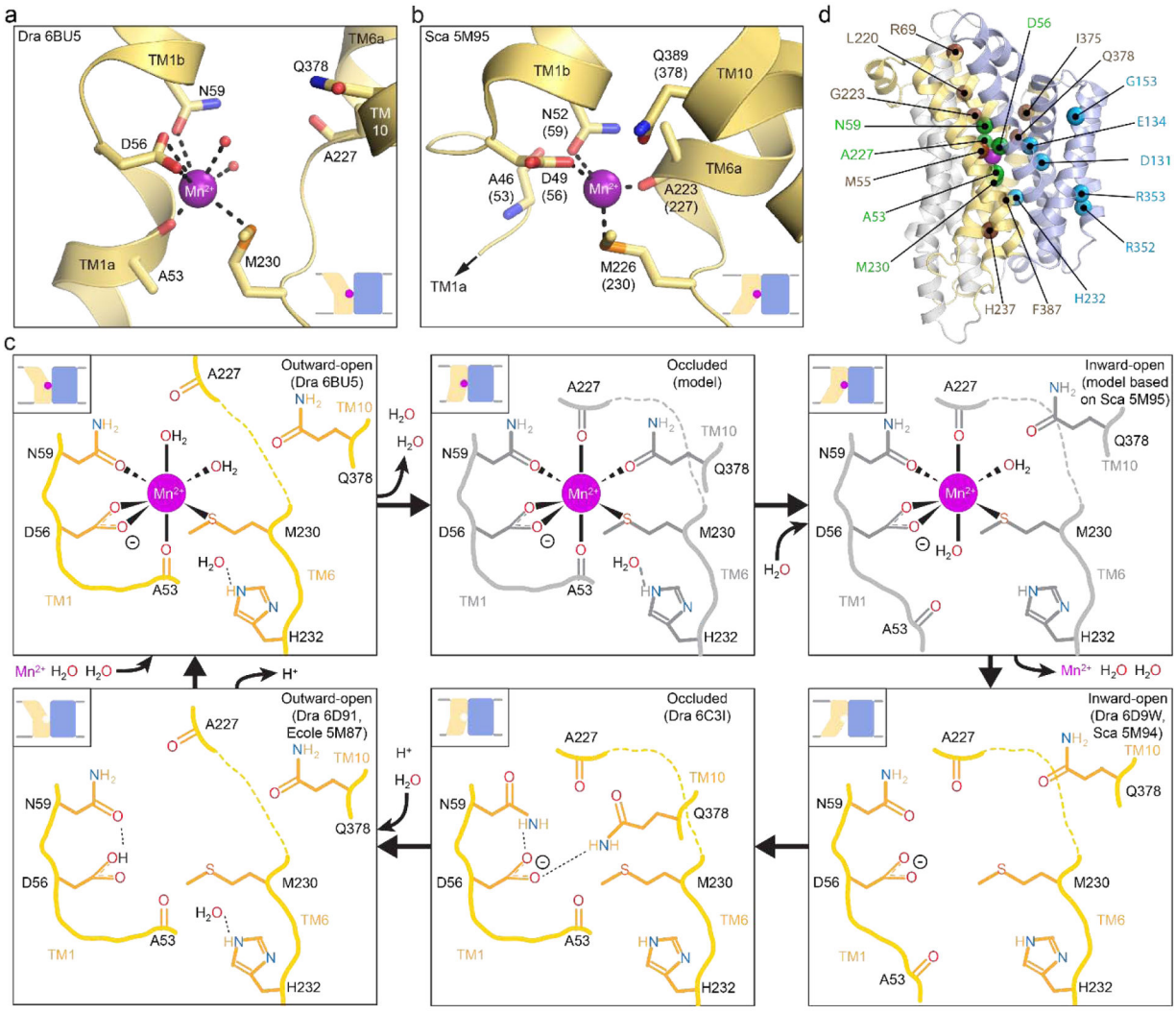

Figure 5. Conserved Nramp binding site changes across conformational states.

(a,b) Structures of outward-open DraNramp (a; PDB ID: 6BU5) and inward-open ScaNramp (b; PDB ID: 5M95; DraNramp residue numbering in parentheses) include bound Mn^{2+} substrate. In the outward-open DraNramp, D56, N59, M230 and the A53 carbonyl, along with two water molecules, coordinate Mn^{2+}, while in the inward-open ScaNramp D56, N59, M230, and the A227 carbonyl coordinate Mn^{2+} (DraNramp residue numbering). (c) Model for changes in the metal-binding site during the transport cycle, including a possible switch from four to six to four metal-binding residues from the outward-open state, through a hypothetical occluded conformation (gray) in which Q378 may coordinate the metal, to the inward-open state. A change in metal coordination could serve to preferentially stabilize the conformational transition state to lower the activation energy barrier to transport. The surrounding binding-site residues may stabilize the negatively charged D56 during the return to the outward-open state, while D56 protonation likely then orients neighboring N59 to optimally bind incoming metal. Model adapted from Bozzi et al. 2019 [136]. (d) Mapped on the outward-open DraNramp structure are the Cα positions of residues from the inner metal

coordination sphere (green), the outer selectivity sphere (brown) or the salt-bridge network (cyan) that influence metal selectivity, as discussed in the text.

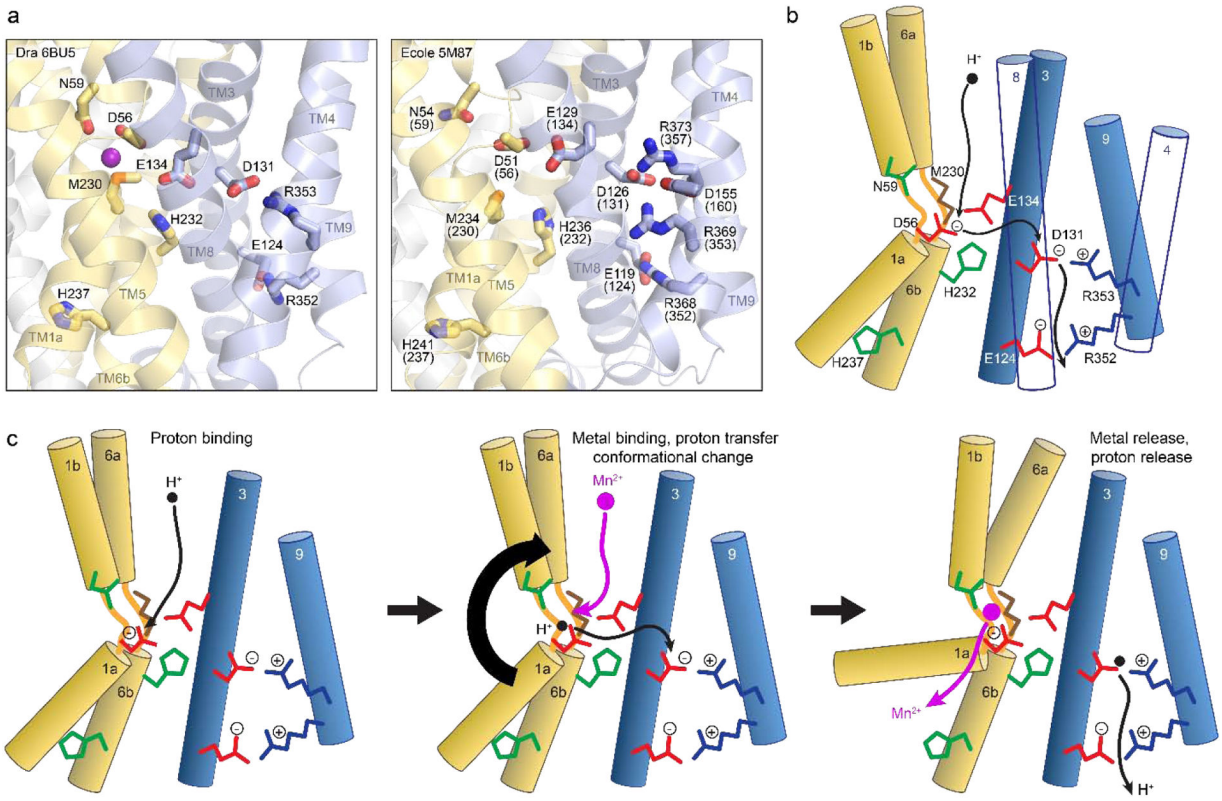

Figure 6 . Conserved hydrophilic network forms Nramp proton-transport pathway.

(a) Structures of outward-open DraNramp (left; PDB ID: 6BU5) and EcoleNramp (right; PDB ID 5M87; DraNramp numbering in parentheses) show conserved network of protonatable residues on TMs 1, 6, 3, and 9 leading from metal-binding site to the cytosol, which is a unique feature of the Nramp-clade of the LeuT-fold family. (b) Model for multistep proton transport in DraNramp based on predicted pK_a values and mutagenesis data. The proton enters through the extracellular vestibule to bind to D56, is transferred to D131, facilitated by H232 and E134, and exits to the cytosol through a narrow passageway between TMs 3, 4, 8, and 9 that includes multiple additional charged and hydrophilic residues. (c) Model for Nramp proton-metal cotransport. (Left) A proton enters the extracellular vestibule and binds to D56. (Middle) Incoming metal displaces the proton as it binds to D56, N59, M230, and the A53 carbonyl. The proton passes to D131, stabilized by H232 and E134 during the transfer. Bulk conformational change occurs as modeled in Figure 3(b), possibly adding TM10's Q378 and TM6's A227 carbonyl to the metal-coordination sphere to drive the rearrangements. (Right) The proton is ultimately released to the cytosol through the TM3-TM9 salt-bridge network, a structural feature which also imparts a voltage dependence to this process that limits metal transport at lower magnitude $\Delta\Psi$. Metal substrate is released into the wide intracellular vestibule and the empty transporter can return to the outward-open state to repeat the cycle. Figure adapted from Bozzi et al. 2019 [132].

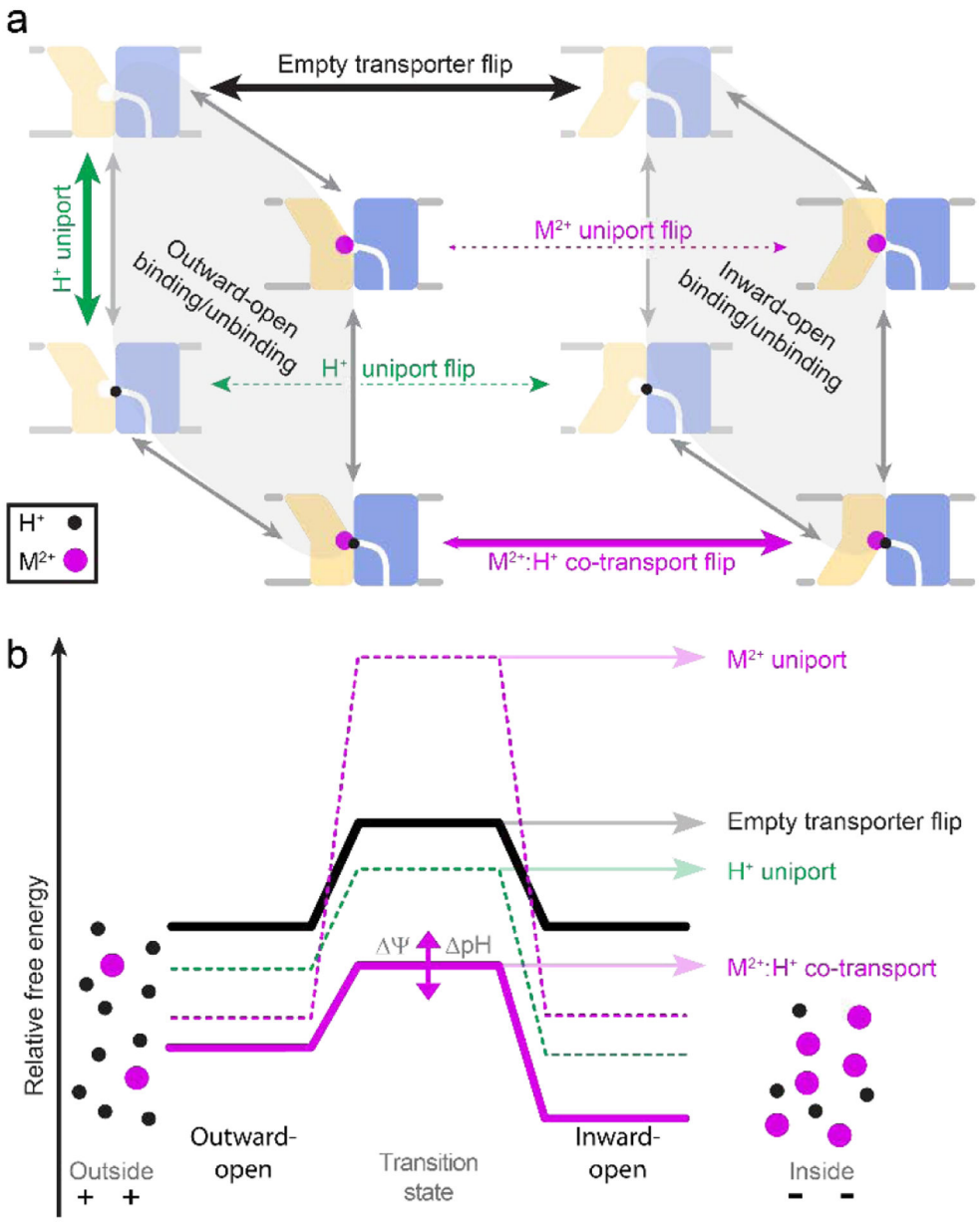

Figure 7. Kinetic model of Nramp metal and proton transport.

(a) Nramp transport cycle diagram illustrating possible binding/unbinding and transport events. While metal transport requires bulk conformational change, proton uniport occurs through the outward-open state. Metal elemental identity controls whether either M^{2+}:H^{+} cotransport (with a stoichiometry that may vary depending on voltage and pH) or M^{2+} uniport occurs. (b) Simplified, hypothetical free energy diagrams for Nramp transport events in a typical physiological context of higher [H^{+}] outside, higher [M^{2+}] inside, and a moderate negative-inside ΔΨ. Proton cotransport may significantly reduce the barrier to M^{2+} transport, although for some metals the kinetic barrier to uniport appears to be lower than that for cotransport. Voltage affects both the magnitude of the energetic barriers for metal transport as well as the relative ΔG for transport, while ΔpH affects the energetic barrier and,

depending on the extent of thermodynamic coupling between metal and proton transport, the relative ΔG. The proposed mechanism for Nramps favors metal forward-transport over back-transport, which implies asymmetric kinetic barriers (and thus likely additional stable intermediate states), which are not shown in this model. Figures adapted from Bozzi et al. 2019 [132].

Table 1.

Crystal structures of bacterial Nramp homologs

PDB ID	Homolog	Conformation	Ligand	Resolution (Å)	Notes	Reference
5M94	ScaNramp	Inward-open	None	3.10	TM1a deletion	[140]
5M95	ScaNramp	Inward-open	Mn^{2+}	3.4	TM1a deletion	[140]
6D9W	DraNramp	Inward-open	None	3.94	Inward-locking mutations	[136]
6D91	DraNramp	Outward-open	None	2.35	G223W outward-locking mutation	[136]
6BU5	DraNramp	Outward-open	Mn^{2+}	2.4	G223W outward-locking mutation	[136]
6C3I	DraNramp	Occluded	None	2.95	G45R disease mutation mimic	[136]
5M87	EcoleNramp	Outward-open	None	3.3	Wildtype	[140]
5M8K	EcoleNramp	Outward-open	None	3.6	E129Q mutation	[140]
5M8J	EcoleNramp	Outward-open	None	3.7	H236A mutation	[140]
5M8A	EcoleNramp	Outward-open	None	3.9	E129A mutation	[140]
6TL2	EcoleNramp	Outward-open	Inhibitor	3.8	Bound to benzyl bis-isothiourea inhibitor	[141]
4WGV	ScaNramp	Inward-open	None	3.10	Superseded by 5M94	[139]
4WGW	ScaNramp	Inward-open	Mn^{2+}	3.4	Superseded by 5M95	[139]
5KTE	DraNramp	Inward-open	None	3.94	Superseded by 6D9W	[134]

Table 2.

Substrate selectivity of mammalian NRAMP2 homologs *

metal	Rat NRAMP2	Mouse NRAMP2	Human NRAMP2
Mn^{2+}	Yes: [100, 154, 155]	Yes: [166]	Yes: [133, 134, 161, 204]
Fe^{2+}	Yes: [17, 74, 75, 100, 155, 163, 165]	Yes: [124, 144, 156, 183, 205]	Yes: [88, 109, 133, 134, 157, 160–162, 164, 168, 204, 206]
Co^{2+}	Yes: [154, 155, 163]	Yes: [26, 156, 183, 205]	Yes: [88, 133, 134, 161]
Ni^{2+}	Yes: [100]		Yes: [161]
Cu^{2+}		No: [167]	No: [161]
Zn^{2+}	Yes: [155, 163] No: [154]		Yes: [161, 162] No: [109]
Cd^{2+}			Yes: [133, 134, 139, 157, 159, 161, 164]
Pb^{2+}	Yes: [165]		No: [164]
Hg^{2+}		Yes: [166]	No: [161]
Ca^{2+}		No: [144]	No: [109, 133, 168]

*Transport of metal substrates (or lack thereof) as reported in referenced studies. Illing et al. also showed that VO^{2+} was transported by human NRAMP2, while Cr^{2+}, Cr^{3+}, Fe^{3+}, Cu^{+}, Ga^{3+}, and VO^{+} were not [161], while Arredondo et al. found that Cu^{+} was transported [167].

Table 3.

K_m values for Nramp homologs, noted here to one significant figure in μM, reported in the indicated references

metal	Rat NRAMP2	Human NRAMP2	Human NRAMP1	*S.c.* Smf1p	EcoliNramp	DraNramp
Mn^{2+}		1 [88] 4 [161]	1 [88]	2 [169]	0.3 [178] 0.3 [145] 0.3 [181] 1 [37]	2 [136] 2 [132] 3 [132]
Fe^{2+}	1 [165] 1 [180] 1 [116] 2 [17] 4 [180]	0.5 [88] 1 [109] 1 [161] 3 [157] 5 [161]	0.5 [88]	2 [74] 5 [169]	100 [37]	200 [132]
Co^{2+}		3 [161]		9 [169]		700 [132] 1000 [132]
Ni^{2+}		10 [161]				
Zn^{2+}	10 [180]	10 [162] 20 [161] 30 [161]	0.6 [94]			30 [132]
Cd^{2+}		0.3 [139] 1 [159] 1 [161]			3 [142] 9 [142]	3 [132] 6 [136] 7[132]
Pb^{2+}	2 [165]					
VO^{2+}		20 [161]				

Additionally, K_m values for Mn^{2+} of 20 μM for EcoleNramp [140] and 0.1 μM for *S.* Typhimurium Nramp [37], and a K_m for Fe^{2+} of 2 μM for mouse NRAMP2 [156], were also reported.

Table 4.

Residue positions that influence metal ion selectivity in Nramps

Location	Residue in DraNramp	TM	Conformation bound to Mn^{2+}	Effect of mutations
primary coordination sphere	A53	1a	outward [136]	NA
	D56	1nh[a]	outward [136] inward [139]	eliminates transport [133, 135, 136, 139, 140, 177, 178, 181, 183]
	N59	1b	outward [136] inward [139]	eliminates transport [133, 135, 136, 139, 140, 177, 178]
	A227	6nh	inward [139]	NA
	M230	6nh	outward [136] inward [139]	alters metal selectivity [71, 132, 133, 136, 186, 188], impairs/eliminates transport [133, 139, 140, 145, 157, 184]
Secondary selectivity sphere	Q378[b]	10	inward (MD simulation) [133, 157]	alters metal selectivity [136], impairs/eliminates transport [135, 157]
	M55	1nh	--	alters metal selectivity [177]
	R69	1b	--	alters metal selectivity [188]
	L220	6a	--	alters metal selectivity [188]
	G223	6a	--	alters metal selectivity [188]
	H237	6b	inward (Zn^{2+} soak) [139]	alters metal selectivity [180, 188]
	I375	10	--	alters metal selectivity [171]
	F387	10	--	alters metal selectivity [171]
salt-bridge network	D131	3	--	alters metal selectivity [132]
	E134	3	--	alters metal selectivity [132]
	G153	4	--	alters metal selectivity [134, 144], impairs transport [124]
	H232	6b	--	alters metal selectivity [132]
	R352	9	--	alters metal selectivity [132]
	R353	9	--	alters metal selectivity [132]

[a] nh is non-helical region

[b] May be part of the primary coordination sphere in some states

Table 5.

Residue positions involved in proton coupling and transport

Location	Residue in DraNramp	TM	approximate pK_a (apo Dra, Sea)	Effect of mutations	Proposed roles
Metal-binding site	D56	1nh[a]	6.5 [136], 7 [157]	eliminates H^+ transport [132, 136, 140, 181]	metal binding, initial H^+ binding, ΔpH stimulation, voltage dependence
	N59	1b	--	alters H^+:M^{2+} stoichiometry [132, 136, 140]	metal binding
	M230	6nh	--	alters H^+:M^{2+} stoichiometry [132, 140], eliminates ΔpH stimulation [132, 140]	metal binding, substrate selectivity, ΔpH stimulation
Metal-release pathway	H237	6b	4 [136], 5 [157]	eliminates H^+-transport [132, 136], alters H^+:M^{2+} stoichiometry [180], shifts ΔpH dependence [183], conformationally-locks transporter [135]	conformational change, metal exit
Proton-transport pathway	E124	3	6 [136], 9 [157]	alters H^+:M^{2+} stoichiometry [132], reduces ΔΨ dependence [132]	voltage dependence, H^+ exit
	D131	3	4.5 [136], 5.5 [157]	eliminates H^+-transport [132, 136, 181], reduces ΔΨ dependence [132]	secondary H^+ binding, voltage dependence
	E134	3	11.5 [136], 10.5 [157]	impairs H^+ transport [132, 136, 157], alters H^+:M^{2+} stoichiometry [140], reduces ΔΨ dependence [132], alters ΔpH stimulation [132, 140, 157]	H^+ transfer, ΔpH stimulation, voltage dependence
	L164	4	--	alters H^+:M^{2+} stoichiometry [163]	helps shape H^+ pathway
	H232	6b	3.5 [136], 4.5 [157]	eliminates H^+-transport [132, 136, 140], eliminates ΔpH stimulation [132, 140], shifts ΔpH dependence [183], conformationally-locks transporter [135]	H^+ transfer, ΔpH stimulation, conformational change
	R352	9	12.5 [136], 15 [157]	alters H^+:M^{2+} stoichiometry [132], reduces ΔΨ dependence [132]	voltage dependence, H^+ exit
	R353	9	12.5 [136], 19 [157]	alters H^+:M^{2+} stoichiometry [132], reduces ΔΨ dependence [132]	voltage dependence, H^+ exit

[a] nh is non-helical region